INFLUENCE OF REPAIR GRINDING ON THE CORROSION RESISTANCE AND CLEANABILITY OF TANK CONTAINERS

T. Ohligschläger[1], V. Roiko-Jokela[2], R. Alén[2], J. Nenonen[3]

[1]Tornio Research Centre, Outokumpu Tornio Works, Finland, [2]University of Jyväskylä, Finland,
[3]Robogrind Oy, Finland

Abstract

Differently prepared surface finishes were investigated to clarify the influence of the grinding procedure on the properties of the inner surfaces of tank containers. The samples were produced either by manual grinding or by a recently developed grinding robot followed by pickling in mixed acid always. Their corrosion resistance was studied by immersion into sodium hydroxide and sulphuric acid solutions as well as into mustard. They were exposed to salt spray and their pitting potentials were measured. The cleanability of the samples was determined after their controlled soiling with milk, red wine, SB latex, oleic acid and carbon black by means of a cleaning simulator. In each case, conditions comparable to those of real tank containers were chosen. The results indicated clear correlations between the cleanability of the samples and their treatment history (i.e., surface preparation and soiling). The influence of the finish on the corrosion resistance of the samples was minor.

Introduction

Tank containers are often used for the transport of liquid bulk chemicals and liquid food products. Normally, the nature of the transported good decides about the material that has to be chosen for the inner shell of the tank container. Stainless steels but also mild carbon steels, which often have to be covered with linings like PTFE, are quite common. Also tanks made of special materials like nickel base alloys, titanium or aluminium are used for particular applications. As tank containers are often run by rental companies who may own huge fleets of vessels, stainless steel grade ASTM 316L is a quite popular material, because its high corrosion resistance assures that the tank is compatible with a huge variety of goods. Normally, a cold rolled, pickled and skin passed 2B mill finish is used due to its excellent cleanability properties.

As it is not possible for the owner of rental tank containers to control all goods that come into contact with his vessels, it is not unusual that the inner shell of the tank is damaged by pitting or general corrosion, which is mostly caused by not suitable loads. In addition, remainders of some transported products may remain on the inside walls of tank containers even after intensive cleaning operation. Latex is a typical example for such a difficult to remove substance. In order to avoid the contamination of the following load, already relatively small corrosion damages like pin holes need to be repaired e.g. by grinding or even welding. Difficult to remove residues have to be removed by intensified cleaning or even grinding. Usually a repair-grinding treatment is followed by fine grinding and mixed acid pickling restoring the excellent corrosion resistance and cleanability properties of the stainless steel surface. After final rinsing, the surface is usually passivated in air.

As the final finish has significant influence on the performance of the repaired tank container, this studied aims to compare the corrosion and cleanability properties of several stainless steel surfaces produced by traditional manual grinding and a newly developed grinding robot.

Experimental

Five different flat samples were prepared by dry grinding a 3 mm thick sheet of grade ASTM 316L. The chemical composition is given in Table 1. Three samples were ground with the grinding robot using grinding belts with different grit sizes (sample codes: *Robo-120grit*, *Robo-240grit* and *Robo-400grit*). Two samples were produced by manual dry grinding, one by a normal standard procedure (sample code: *Man-normal*) and another one by an enhanced procedure applying an additional refining treatment giving the surface a non-unidirectional final finish (sample code: *Man-refined*). In all cases, attention was paid not to overheat the sample surface by excessive grinding pressure. For comparison, the original cold rolled, pickled and skin-passed 2B finish was included in the test program (sample code: *2B-pickled*). All samples were subjected to pickling in stirred mixed acid containing 20 w-% HNO_3 and 2 w-% HF at 23°C for about 90 min reflecting conditions used in tank container refurbishment.

Table 1. Chemical composition of the sample material of stainless steel grade ASTM 316L given in w-%.

C	Si	Mn	Cr	Ni	Mo	N	Fe
0.022	0.52	1.66	16.7	10.7	2.58	0.047	Balance

The surface roughness of the samples was measured according to ISO 4287 and 4288 perpendicular to the grinding or rolling direction. Their reflectivity was determined at an incident angle of 60° in accordance with ISO 2813 longitudinal ($R60_{long}$) and transversal ($R60_{trans}$) to the grinding or rolling direction of the samples. The results are given in dimensionless gloss values with reference to the commonly used dark glass standard. The directionality $DIR60 = R60_{long} / R60_{trans}$ was calculated [1]. Images of the surfaces were taken with an optical profilometer using vertical scanning interferometry. All surface characterisations were performed before and after pickling.

The resistance of the pickled samples against general corrosion was compared by immersion in 20% naturally aerated H_2SO_4 at 40°C, in 40% NaOH at 90°C and in 40°C warm mustard, which contained 2.9 w-% NaCl according to the producer. The corrosion rate was calculated after 30 days on the basis of the measured weight loss. The pitting potentials at 10 $\mu A/cm^2$ were determined in naturally aerated 0.2 M NaCl solution before and after pickling. The measurements were performed potentiodynamically with a scan rate of 20 mV/min at 22°C in flush-port cells as described in ASTM G150. The electrochemical active electrode area was about 1 cm^2. The averages of six measurements are reported against the used KCl saturated calomel reference electrodes (SCE). Finally, a cyclic salt spray test was performed at 35°C for 500h spraying a 5 w-% $CaCl_2$-solution for 5 min into the chamber and allowing 55 min to dry.

Cleaning tests with oleic acid, milk, red wine (blend of 63% Cabernet Sauvignon and 37% Merlot, 13.7% alcohol), SB-latex and carbon black were performed using the cleaning simulator developed in the Laboratory of Applied Chemistry of the University of Jyväskylä, Finland [2]. Before each cleaning test, the samples were initially cleaned with a 45°C warm alkaline cleaning solution and then rinsed with warm tap water and ethanol before air-drying. A suspension of oleic acid in ethanol, milk and a suspension of carbon black in ethanol were sprayed with the cleaning simulator onto the samples. Red wine and latex were spread on the samples by sinking them into the soiling fluids and lifting them up after a certain period of time for drying in near vertical position. The samples were then cleaned by spraying a solution of a weakly alkaline cleaning agent in medium hard water (6º dH) onto the samples along the lay of the surfaces. For oleic acid, a concentration of 0.5 vol.-% was chosen, for carbon black 3 vol.-% and for milk and red wine 1 vol.-%. The latex soil was removed only with tap water. Measuring the samples with a machine vision system [3] before and after each cleaning run allowed calculating the achieved cleaning percentage (C-%) according to equation (1) taken from ASTM D5343:

$$C-\% = \frac{R_C - R_S}{R_0 - R_S} \cdot 100\% \, , \tag{1}$$

where R_C is the measurement values of the cleaned plate, R_S the values of the soiled plate and R_0 the result of the pre-cleaned sample. The average values of 12 samples originating from 3 test runs for each soil are reported and used for ranking.

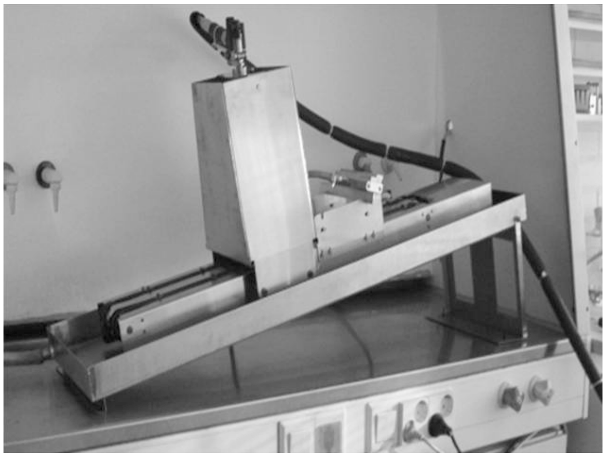

Figure 1. Cleaning simulator developed in the Laboratory of Applied Chemistry of the University of Jyväskylä [2].

Results and Discussion

The results of the surface characterisations are presented in Table 2. Images of the surface profiles of all pickled samples and of some selected unpickled ones can be found in Figure 2.

Table 2. Results of the surface characterisations before and after pickling. Ra and Rz are calculated according to ISO 4287 and 4288. The reflectivity is given in gloss values. DIR60 is dimensionless. The surface roughness of sample *Man-refined* was measured perpendicular to the initial grinding direction. As this sample was not as homogenous as the others, its reflectivity varies locally so that calculated DIR60 values would not be meaningful.

Sample	Before pickling					After pickling				
	Ra / µm	Rz / µm	$R60_{long}$	$R60_{trans}$	DIR60	Ra / µm	Rz / µm	$R60_{long}$	$R60_{trans}$	DIR60
Robo-120grit	1.55	8.26	119	18	6.61	1.30	6.89	105	21	5.00
Robo-240grit	0.78	4.68	138	24	5.75	0.76	4.57	120	25	4.80
Robo-400grit	0.39	2.61	193	41	4.71	0.36	2.21	154	41	3.76
Man-normal	2.34	9.70	119	22	5.41	2.13	9.57	131	32	4.09
Man-refined	1.49	6.16	61-73	86-137	-	1.80	7.58	80-84	83-116	-
2B-pickled	0.08	0.41	197	176	1.12	0.14	0.84	31	30	1.03

As expected, the roughness and reflectivity values for the surfaces made with robot depended clearly on the used grit size (see Table 2). The manually ground surfaces showed relatively rough surface finishes. The low variation between measurements taken at different spots of the surfaces made by the robot compared to manual grinding emphasises the superior reproducibility and precision of the grinding robot. After pickling, the roughness and especially the reflectivity along the grinding direction of the samples produced by the robot decreased while the roughness of the manually ground finishes and of the 2B surface remained on a similar level or even increased. As a comparison with the images presented in Figure 2 shows, the shape of the surfaces became rounder and formerly present pocket like structures were removed. In the case of the 2B finish, the surface was clearly over-pickled after pickling resulting in low reflectivity values.

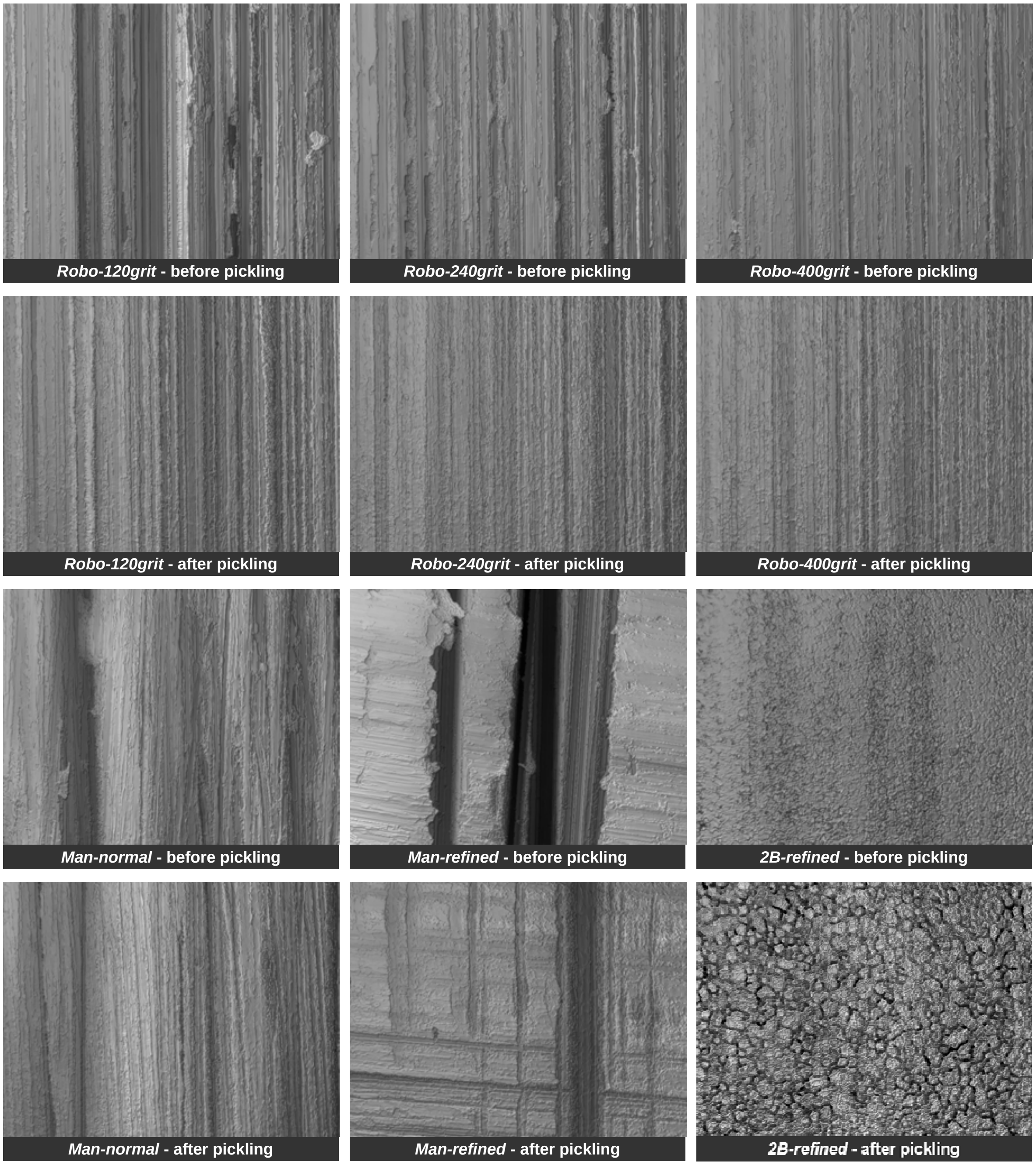

Figure 2. Profilometer images of the samples before and after pickling. The image size is 299 x 226 µm. The grey shade represents the height information of the recorded profile. The height scale was the same for all samples except for the relatively smooth sample *2B-pickled*, where a five times smaller scale was used. The images illustrate the effect of strong mixed acid pickling on stainless steel surfaces. The reduction of surface details like burrs and pockets as well as the widening of the grain boundaries on sample *2B-pickled* can be recognized.

The corrosion rates measured for all samples in H_2SO_4, NaOH and mustard showed no significant differences. An influence of the surface finish was not found. No local attack was observed on any sample. A corrosion rate of 0.34 mm/a was determined in the 40°C warm 20 w-%

H_2SO_4, which is in good agreement with published handbook data [4]. All samples showed a dull surface after testing. Especially grinding grooves on surfaces that had been treated by the robot were less expressed. After the tests in 90°C hot 40 w-% NaOH as well as in 40°C warm mustard, no significant corrosion attack had taken place on any sample as the corrosion rates were in all cases below 0.01 mm/a. Nevertheless, the samples were a little bit duller than before and a slight, partly inhomogeneous darkening was observed. The appearance of the grooves was not significantly changed in any case. The results were better than expected from handbook data [4] and may be attributed to advances in steel making during the last decades.

Table 3. Pitting potentials vs. SCE in 0.2M NaCl solution at room temperature before and after pickling. The mean value of 6 measurements and its confidence with a probability 95% is given. Higher pitting potentials correspond to better resistance against localised corrosion. Differences between samples that are lower than about 30 to 40 mV can usually be neglected due to the stochastic character of pitting corrosion. The relatively low value for the as received 2B finish might be related to some slight chromium depletion in the surface layer of the stainless steel sheet caused by the annealing processes.

	Robo-120grit	*Robo-240grit*	*Robo-400grit*	*Man-normal*	*Man-refined*	*2B-pickled*
As received	551 ± 13 mV	517 ± 11 mV	542 ± 24 mV	459 ± 56 mV	481 ± 15 mV	464 ± 8 mV
Pickled	513 ± 15 mV	521 ± 15 mV	519 ± 14 mV	509 ± 11 mV	514 ± 9 mV	516 ± 13 mV

As can be seen from Table 3, the pitting potentials of unpickled surfaces prepared by the grinding robot are higher than the ones measured for the 2B mill finish and the unpickled manually ground samples. This indicates that it is possible to produce highly corrosion resistant finishes with the grinding robot. After pickling, however, all values are on the same level demonstrating the strong influence of pickling on the corrosion resistance of stainless steels.

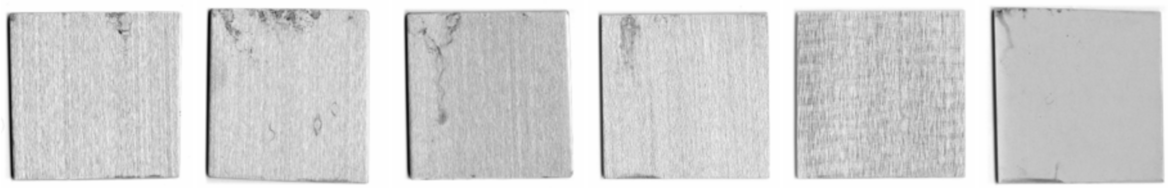

Robo-120grit ***Robo-240grit*** ***Robo-400grit*** ***Man-normal*** ***Man-refined*** ***2B-pickled***

Figure 3. Photographic images of the samples after the salt spray test. A relatively small sample size of about 45 x 45 mm was chosen to simplify sample preparation with the grinding robot. The orientation of the samples in the images corresponds to their orientation in the salt spray chamber. Red rust from corrosion attack can be recognized as dark areas on the sample surfaces.

Images of the samples after salt spray testing are presented in Figure 3. The degree of rusting on the samples did not correspond to measured surface roughness parameters. The *2B-pickled* and the *Man-refined* sample performed best. Most corrosion attack started at the edges of the samples despite careful edge preparation before testing.

Table 4. Results of the cleaning tests with 5 different soils as cleaning percentages and resulting relative ranking of the tested surface finishes. The mean value of 12 single measurements and its confidence with a probability 95% is given. The rank *1* indicates the best results and the rank *6* the worst result with each soil.

	Robo-120grit		*Robo-240grit*		*Robo-400grit*		*Man-normal*		*Man-refined*		*2B-pickled*	
Oleic acid	37 ± 10 %	3	31 ± 8 %	6	40 ± 9 %	1	35 ± 10 %	5	40 ± 10 %	1	36 ± 7 %	4
Milk	27 ± 2 %	2	27 ± 2 %	2	23 ± 1 %	6	24 ± 2 %	5	26 ± 3 %	4	30 ± 2 %	1
Red wine	43 ± 4 %	4	45 ± 3 %	2	45 ± 5 %	2	43 ± 6 %	4	40 ± 5 %	6	51 ± 6 %	1
SB-latex	20 ± 4 %	2	15 ± 4 %	4	8 ± 3 %	6	18 ± 7 %	3	21 ± 2 %	1	12 ± 3 %	5
Carbon black	55 ± 10 %	2	44 ± 6 %	5	39 ± 10 %	6	64 ± 7 %	1	52 ± 7 %	3	49 ± 3 %	4
Average rank	2.6		3.8		4.2		3.6		3.0		3.0	

Table 4 summarizes the results of the cleaning tests. As can be seen from the cleaning percentage values, the influence of the different soils on the cleaning test results was stronger than the influence of the studied surface finishes. Therefore, a ranking system that considered the results of the different surfaces with each soil had to be applied to compare the performance of the differently prepared finishes. The best average rank was reached by sample *Robo-120grit*, which did not achieve the best cleaning performance with any applied soil. The samples *Man-refined* and *2B-pickled* gave also quite good overall-results reaching the highest rank in two categories but also being relatively difficult to clean from some other soils. The samples *Robo-240grit*, *Robo-400grit* and *Man-normal* could cope relatively well with only a few soils but were more difficult to clean from others.

The averaged results of all cleaning tests did not correspond to the surface roughness of the samples, as the relatively rough finish *Robo-120grit* gave the best overall-performance followed by the very smooth *2B-pickled* finish and the relatively rough *Man-refined* surface. The removal of some soils, namely oleic acid and red wine, however, did follow the surface roughness values while cleaning of milk, SB-latex and carbon black was obviously more influenced by other surface properties.

Conclusion

The properties of the prepared finishes resembling surfaces found in refurbished tank containers are not only defined by the used grinding process but also influenced by the applied final mixed acid pickling. Their resistance against general and localised corrosion under conditions of continuous immersion does not significantly depend on the applied surface treatment. As the tests in the cleaning simulator have proven, the cleaning result depends more on the type of soil than on simple surface roughness parameters like Ra or Rz values. Several surfaces could cope well with some of the applied soils while being difficult to clean from the others soils. The surface with the best all-round properties was the roughest finish produced by the grinding robot.

Acknowledgements

The ground samples were carefully prepared by the inventor of the grinding robot, Mr R. Siipo, Siipotec Oy, Finland and by Mr B. de Bos, Robogrind Services babv, Belgium. The authors wish to thank Mr G. Woods, Technical Secretary of the International Tank Container Organisation (ITCO), for the fruitful discussions.

References

[1] T. Taulavuori, J. Koskiniemi: Proceedings of the 4th European Stainless Steel Science and Market Conference, 2nd Vol., French Iron and Steel Technical Association, Paris, 2002, pp. 260-263

[2] T. Suontamo: “Development of a Test Method for Evaluating the Cleaning Efficiency of Hard-Surface Cleaning Agents”, Doctoral Thesis, University of Jyväskylä, Jyväskylä, 2004

[3] V. Roiko-Jokela, R. Alén, T. Suontamo, and H. Salo: “New detection methods for the cleanability test of hard surfaces”, Book of Abstracts NCSS-5, Fifth Nordic Conference on Surface Science, Tampere, 2004, pp. 36-37

[4] Outokumpu Stainless Steel Oy, Outokumpu Stainless Corrosion Handbook, 9th ed., Espoo, 2004

REWEAR AND CHEMICAL RESISTANCE OF SOL-GEL COATINGS ON STAINLESS STEEL SUBSTRATE

T. Vuorio[1], J. Jaakkola[2], M. Kolari[3], J. Mannila[4], J. Nikkola[4], X.W. Liu[2], O. Söderberg[2],
A. Mahiout[4], S-P. Hannula[2]

[1]HAMK University of Applied Sciences, Finland, [2] Helsinki University of Technology, Finland,
[3]Millidyne Oy, Finland, [4] VTT Technical Research Centre of Finland, Finland

Abstract

Despite of their excellent corrosion resistance it is advantageous to protect also the stainless steels surface from staining and finger prints in many household applications. This may be carried out with sol-gel based hybrid coatings. They can be tailored according to the demands of their service environment by controlling the amount~~s~~ and composition of the ceramics and polymer constituents of the coating. These hybrid coatings can be readily applied on ordinary stainless steel (e.g., EN 1.4301/AISI 304). As increasing amount of stainless steel products is used in domestic applications, information concerning the chemical resistance of the applied coatings against the household chemicals is useful when designing for the best possible coating solutions. These surfaces should also tolerate certain types of wear.

In this work a small-scale study on the resistance of coated stainless steel surfaces against typical household chemicals were performed. Experiments were carried out using immersion and droplet exposure corrosion testing as well as wear testing by applying household cleaning liquids with brushing. The chemicals applied varied from chlorides to alkaline mixtures. Studied transparent SiO_2-based sol-gel coatings were from 100 to 300 nm in thickness. By changing the organic and inorganic counterparts of which the latter one forms the network acting as a backbone of the coating, a clear difference of the resistance of the coatings was obtained. While applying mainly inorganic components, the wear resistance of the surface was superior in comparison to the other studied coatings – and similarly, when the amount of the polymeric counterpart was major, the chemical resistance could be increased. For the practical applications one should find the best combination of these two.

Introduction

Steel may obtain improved corrosion resistance connected to the selected functional properties such as hydrophobicity, with organosilica coatings by varying the composition of precursors[1,2]. In these hybrid coatings, ormocers (organically modified ceramics), the inorganic component enhances durability, scratch resistance and adhesion to the metal substrate, while the organic components grant flexibility and density of the coating[3]. Process parameters influence a lot to the properties of the final surface. For example, higher silica content gives smooth and uniform surface, while increasing alcohol in the sol results in porosity, larger effective surface area and contact angle, e.g., hydrophobicity[4]. Aging of the sol may prevent formation of a dense coating[5].

The present study concerns stainless steel used in household surface applications, where the one of the main interests is cleanability. Stainless steels commonly used in the food sector have surface energies around 40 mN/m. While to reduce the tendency of attachment of bacteria and milk proteins, the surface energy level should be lowered to about 25 mN/m, which is reachable for example with the sol-gel coated stainless steel AISI316T[6]. In addition to the surface energy there are several factors affecting the suitability and tolerance of the surface to be cleaned. Usually cleaning is carried out with some kind of mechanical removal method that may cause wear of the surface. Such wear studies especially on coatings with stainless steel substrate are rare[7]. Also, the chemical resistance of the coatings to the cleaners is important. The most important components from the cleaners include tensides, softeners, solvents and, depending on the soil to be removed, alkalis or acids[8]. The silica based sol-gel coatings do resist oxidation and corrosion under acidic conditions or when elevated chloride activities are present[3]. This is also shown in the corrosion studies of AISI 304 steels with hybrid silica sol-gel coatings in marine water[9-11], in HCl[10], and in H_2SO_4 solution[11]. Here, the coating should exceed certain minimum thickness to be effective enough. Since there is not much information how the hybrid silica based sol-gel coatings tolerate the household chemicals, the present study is focused in this subject.

Experimental

Five silica based sol-gel coatings with varying ceramic/polymeric compositions were applied on the AISI 304 (2B or 2J) substrate. The sprayed coatings were thicker than the dipped ones and Coating C was clearly thinner than all the others.

Hardness of the coatings on 2B surfaces was tested by the HV0.3 microhardness measurement with Zwick & Co Z323 (EN-ISO 6507). To get more insights of the properties in sub-microscale, nanoindentation was implemented on Coating B on 2B substrate, for three locations representing typical features of the coating surface (Figure 2). Here, TriboIndenter® nanomechanical test system (Hysitron, Inc.) was utilized with a Berkovich tip (130 nm top radius). The maximum load of the indentation cycle was set at 700 µN, and loading-holding-unloading at 70 µN/s-5 s-70 µN/s. A rapid unloading test at 350 µN/s (Location 3) was performed to verify the indentation-creep effect on the measured mechanical properties, which is significant on soft materials[12,13]. All together 8, 10 and 19 indents were performed at Location 1, 2 and 3, respectively. Hardness and modulus values were extracted by analyzing the unloading part of the load-depth curve following the Oliver-Pharr scheme[14].

The wear resistance was studied with coatings on the AISI 304 2J substrates at the ambient temperature with the laboratory made apparatus. The rougher substrate condition was chosen to detect better the surface wear. The wear head was rotating with a constant speed and the load was 100 g/cm^2. The wear part was either of household PataPata™ steel wool or soft cloth soaked to abrasive liquid containing hard particles (household cleaner Cif™ or water with Al_2O_3). At certain number of the rotation cycles the sample was rinsed clean, observed visually, photographed and its hydrophobic properties were studied with a droplet of water. The test was stopped when the coating was clearly worn and the surface morphology was examined with visual observation and scanning electron microscopy (SEM).

Immersion tests of the coatings on the smooth 2B substrates were carried out at 30°C in the water solutions of the common household cleaners: Tolu™ (solution pH 9), Fairy™ (solution pH 8) and Andy™ (solution pH 7). The weight change and visible surface changes were measured and recorded during and after the tests. The effect of contact angle with water in the immersion test was studied for those samples immersed in Tolu™- or Andy™-solutions. The contact angles were measured in Millidyne Oy.

The droplet exposure corrosion tests were carried out with the coated samples both with the smooth 2B and with the brushed 2J substrate. Here, the undiluted chemical, Klorin (pH 13), Cif (pH 4) or Ajax (pH 7), was applied with pipette to filter papers (diam. 10 mm) on specimen surface. Glass covers (Ø 24 mm) were placed on these papers to prevent evaporation of the chemicals during the exposure of 1 h, 3 h, 5 h and 24 h. The samples were studied visually.

Results and Discussion

Hardness, the results of the immersion tests as well as the droplet exposure corrosion tests are collected in Table 1. More detailed discussion of the results is given below.

Table 1. Hardness, the results of the immersion tests as well as the droplet exposure corrosion tests.

	Coating A sprayed	Coating B sprayed	Coating C dipped	Coating D dipped	Coating E dipped
Hardness HV0.3 (transf. to GPa with factor 0.009807)	91 ± 4.5 (0.9±0.04)	186 ± 38.6 (1.8±0.38)	247 ± 17.4 (2.4±0.17)	251 ± 19.5 (2.5±0.19)	247 ± 19.2 (2.4±0.19)
Weight change (mg)					
– after in Tolu™ solution pH9, 337 h	-1.5	-3.9	-1.0	-1.8	-1.6
- after in Andy™ solution, pH7, 338 h	+2.8	+2.7	+1.3	+1.9	+ 1.4
- after in Fairy™ solution, pH8, 383 h	-0.4	-0.3	-0.4	-0.1	-0.9
Contact angle with water					
- original value	65	98 ±	101	94	96
-after Tolu™ solution immersion	56 ± 1.7	74 ± 0.6	94 ± 0.6	94 ± 1.0	80 ± 0.6
-after Andy™ solution immersion	48 ± 2.1	78 ± 0.6	97 ± 1.5	92 ± 1.0	87 ± 1.5
Droplet exposure corrosion testing *					
- Klorin™ pH13 24h	2	4	0	0	4
- Cif™ pH4 24h	1	0	0	0	0
- Ajax™ pH7 24h	1	0	0	0	0

* 0 = no change, 1 = small change, 2 = more changes, 3 = additional changes, 4 = much changes, 5 = total removal

Resistance to the household chemicals

The material losses of the coatings in the immersion tests were small in Tolu™ and Fairy™ solutions, but in neutral Andy™ solution they gained some weight. As the material loss in Fairy™ solution was so minimal, the contact angles of these samples were not measured. Only, Coating C restored its hydrophobic properties nearly the same after the other immersion tests. For other coatings there was a clear decrease of the contact angles. In the droplet exposure corrosion test Coatings C and D showed good resistance to Klorin™, a very alkaline and chloride containing cleaner. Nearly all the coatings tolerated also well the acidic Cif™ and neutral Ajax™ solutions with Coating A being the only exception that was clearly attacked.

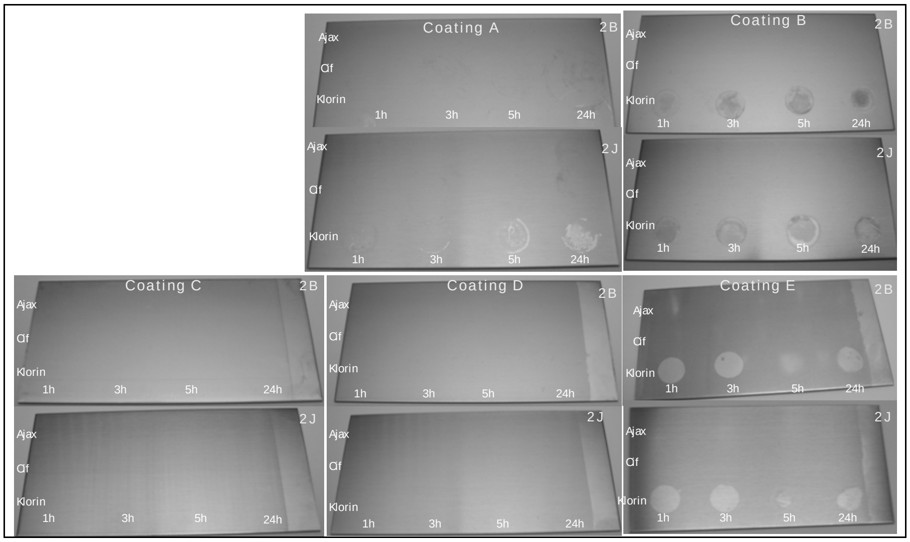

Figure 1. Coated surfaces after the droplet exposure corrosion tests.

Mechanical properties and wear resistance

The hardness value of the AISI 304 (2B) substrate was HV0.3 223 ± 11.9. The values of the thicker sprayed coatings were clearly smaller pointing to their polymeric nature, though of these two coatings more inorganic components bring maybe more hardness to Coating B. The hardness values of the thin dipped coatings were close to each other, and main part of the hardness value coming from the substrate. Maybe Coating D is a bit harder than the others.

Nanoindentation

The results show at micro-scale that the coating is relatively even, indicated by the consistence of the overlaid load-depth plots (Figure 2). However, there is a fluctuation of mechanical properties over the coating (Hardness: 4.4 to 7.9 GPa, Modulus: 0.48 to 0.86 GPa). This fluctuation may have a link to the constitutional/structural variations of the coating. The coating properties obtained from the rapid unloading data show insignificant effect of creep on the accuracy of indentation hardness and modulus, suggesting that the results are reliable.

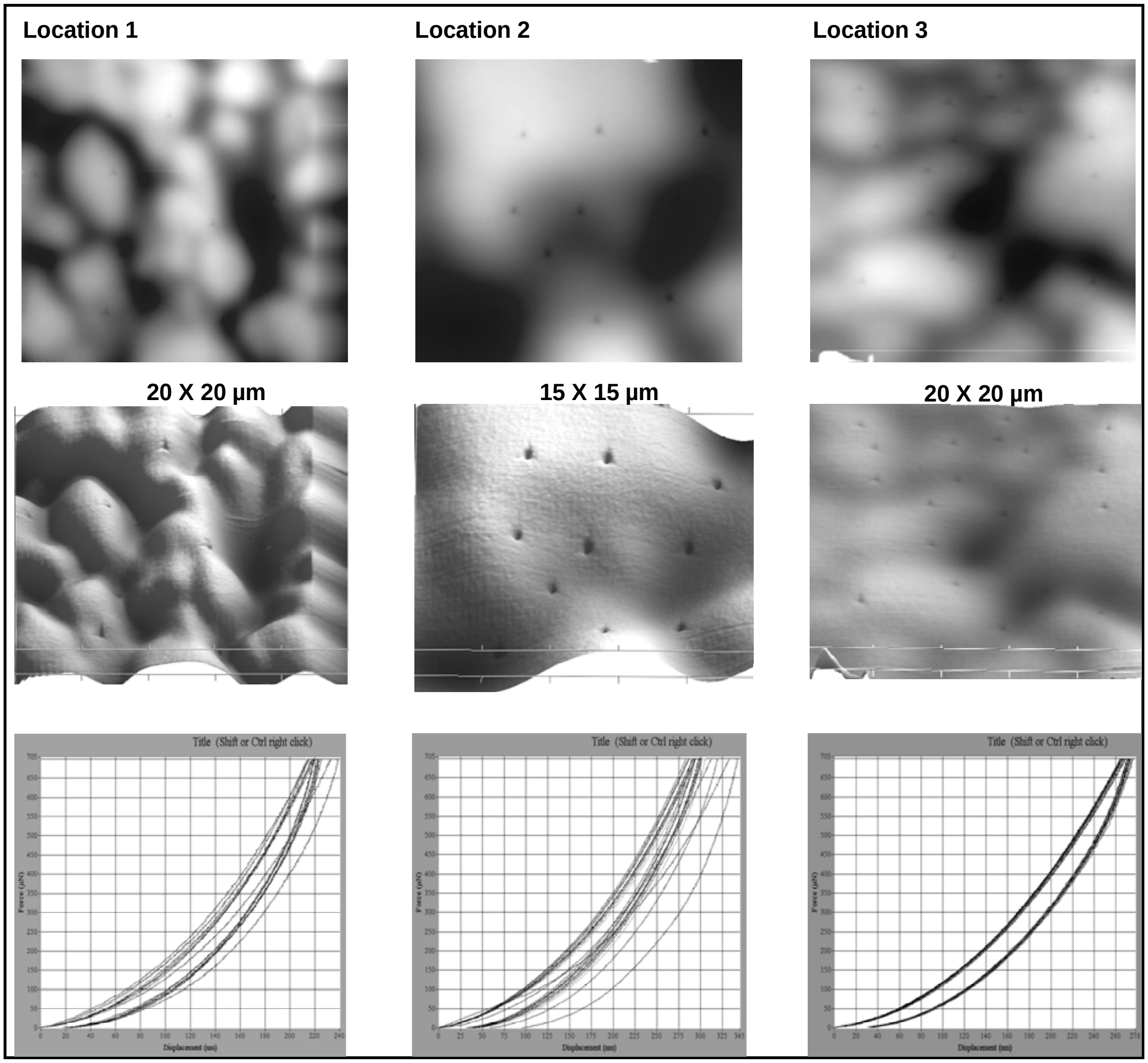

Figure 2. Three nanoindentation locations on Coating B. The first and second row show the 1D and 3D SPM images at the three locations, the third row is the overlaid plots of load-depth (scales µN-nm) of the indentation events at each location.

Wear tests

The studied surfaces wore most in PataPata™ tests which were stopped after 200 rotations. Grinding with alumina resulted in the loss of hydrophobic properties of the coatings which can be seen as a large size of the water droplet on the worn surface in Figure 3. CIF™ wore mainly the coatings while the other wear medium influenced also the substrate below the coatings.

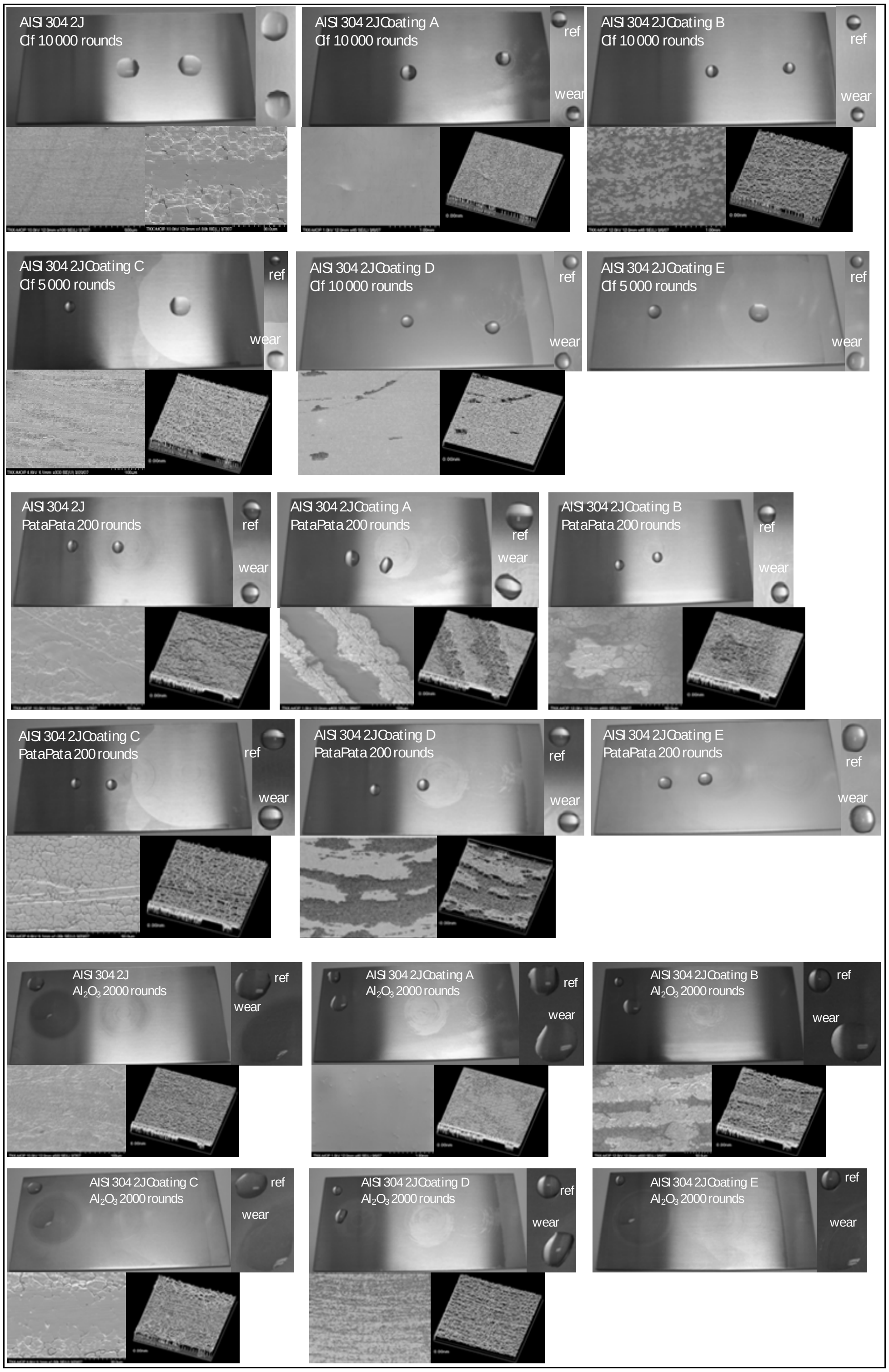

Figure 3. Results of the wear testing: water drop testing of the final wear surface and the reference surface, SEM picture of the wear surface and an oblique picture of the same to show the topography more clearly.

Conclusions

The studied coatings tolerated generally well the domestic chemicals, though the alkaline chloride containing cleaner was devastating to others but Coatings C and D. Also, severe wear resulted in from the wire brush type abrasion, but the conventional cleaning powder liquid they tolerated well. Abrasion with alumina decreased the hydrophobic properties clearly. By tailoring the composition of the sol-gel coating one can produce coatings with sol-gel technique that are wear resistant (Coatings A, B and E) or hydrophobic corrosion resistant (Coatings C and D). Nanoindentation of the Coating B showed fluctuation of the mechanical properties to some extent, though in microscale it seemed to be rather equable.

Acknowledgements

The study has been carried out in co-operation with the Clean and Environmentally Friendly Metal Products - PUHTEET- project. Special thanks belong to VTT Technical Research Centre of Finland and Millidyne Oy for supplying the materials.

References

[1] D.C. Bakul, X.K. Hu, Y. Devaraj, S.K. Dhali: “Sol–Gel-derived corrosion-protection coatings”, Journal of Sol-Gel Science and Technology 32, 1-3, 2004, pp. 143–147.

[2] R. Mahlberg, J. Mannila, J. Romu, J. Nikkola, R. Ilola, O. Söderberg, J. Koskinen, S.-P. Hannula, A. Mahiout: ”Soil resistant and self-cleaning surfaces of stainless steel with new sol-gel and ald coatings”, the 6th European Stainless Steel Conference.

[3] T.L. Metroke, R.L. Parkhill, E.T. Knobbe: “Passivation of metal alloys using sol–gel-derived materials — a review”, Progress in Organic Coatings 41, 4, 2001, pp. 233–238.

[4] S.D. Bhagat, Y.-H. Kim, Y.-S. Ahn: “Room temperature synthesis of water repellent silica coatings by the dip coat technique”, Applied Surface Science, 253, 4, 2006, pp. 2217–2221.

[5] T.P. Chou, C. Chandrasekaran, S.J. Limmer, S. Seraji, Y. Wu, M.J. Forbess, C. Nguyen, G.Z. Cao: “Organic-inorganic hybrid coatings fo corrosion protection”, Journal of Non-Crystalline Solids 290, 2-3, 2001, pp. 153– 162.

[6] P. Saikhwan, T. Geddert, W. Augustin, S. Scholl, W.R. Paterson, D.I. Wilson: “Effect of surface treatment on cleaning of a model food soil”, Surface and Coatings Technology 201, 3-4, 2006, pp. 943–951.

[7] T. Vuorio: Effect of Pretreatments and Type of the Coating on Protective Sol-Gel-Coatings, Master's thesis, Helsinki University of Technology 2005. 129 p.

[8] T. Suontamo: Development of a test method for evaluating the cleaning efficiency of hard-surface clening agents (Department of Chemistry, University of Jyväskylä, Research Report No. 109), Jyväskylä Finland, 2004.

[9] Y. Castro, B. Ferrari, R. Moreno, A. Durán: “Coatings produced by electrophoretic deposition from nano-particulate silica sol–gel suspensions”, Surface and Coatings Technology 182, 2-3, 2004, pp. 199–203.

[10] Y. Castro, B. Ferrari, R. Moreno, A. Durán: “Corrosion behaviour of silica hybrid coatings produced from basic catalysed particulate sols by dipping and EPD”, Surface and Coatings Technology 191, 2-3, 2005, pp. 228– 235.

[11] D.C.L. Vasconcelos, J.A.N. Carvalho, M. Mantel, W.L. Vasconcelos: “Corrosion resistance of stainless steel coated with sol-gel silica”, Journal of Non-Crystalline Solids, 273, 1-3, 2000, pp. 135-139.

[12] G. Feng, A.H.W. Ngan: “Effect of creep and thermal drift on modulus measurement using depth-sensing indentation”, Journal of Materials Research 17, 3, March 2002, pp. 660-668.

[13] B. Tang, A.H.W. Ngan: "Accurate measurement of tip-sample contact-size during nanoindentation of viscoelastic materials", Journal of Materials Research 18, 5, May 2003, pp. 1141-1148.
[14] W.C. Oliver, G.M. Pharr: "An improved technique for determining hardness and elastic modulus using load and displacement sensing indentation experiments, Journal of Materials Research 7, 1992, pp. 1456-1583.

SOIL RESISTANT AND SELF-CLEANING SURFACES OF STAINLESS STEEL WITH NEW SOL-GEL AND ALD COATINGS

R. Mahlberg[1], J. Mannila[1], J. Romu[2], J. Nikkola[1], R. Ilola[2], O. Söderberg[2],
J. Koskinen[1], S-P. Hannula[1,2], A. Mahiout[1]

[1]VTT Technical Research Centre of Finland, Finland, [2]Helsinki University of Technology, Finland

Abstract

Corrosion, fouling and wearing of metal surfaces are the most common problems that are faced in industry as well as in environmental use. In particular, the maintenance of metal products and also the decrease in their value in use can cause major financial losses for example in construction, transportation, process and food industry. Different coatings or surface treatments have been used to enhance the protection properties of metal surfaces. Especially during the last ten years there has been a general interest to study the potential of nanoscale inorganic-organic hybrid sol-gel coatings and ALD coatings to improve the properties of metal surfaces. Typically, sol-gel and ALD coatings are thin, ranging from nanometer scale to several micrometers. Sol-gel coatings are usually optically transparent reminding of very thin layers of varnish or lacquer. The main difference is that the sol-gel coatings consist of an inorganic network, which forms the backbone of the coating. In hybrid sol-gel-coatings, the amount of the organic constituent can be varied according to the application. By changing the organic and inorganic counterparts and varying their amounts, the properties of the coatings can be modified in a wide scale. TiO_2-based or -doped coatings can be photocatalytically active and have self-cleaning properties under UV irradiation. This paper shows how the quality of metal products is improved by applying new thin coatings prepared with ALD or sol-gel techniques. TiO_2-modified sol-gel and ALD coatings were used on stainless steel substrates (EN 1.4301 (AISI 304)) with the dry-brushed (2J) surface finish to enhance the soil resistance and cleanliness level of the material.

Introduction

Stainless steels/Metals are increasingly applied in construction and different process applications. However, the performance and appearance of metal surfaces are often impaired by corrosion, fouling and wear. Environmental factors such as moisture combined with salts, acidic substances or other impurities and dirt particles are responsible for the wear and corrosion of metal surfaces in outdoor use. Fingerprints on metal surfaces of interior products are an annoyance and may generate corrosion/wear as such or indirectly as a result of frequent harsh cleaning (strong chemicals, rubbing). Recently, stainless steel has gained popularity as decorative elements in household applications and in public buildings. This has urged the need for finding easy-to-clean or self-cleaning coatings for these surfaces.

The photocatalytic titanium dioxide (TiO_2) was introduced as a powerful agent in self-cleaning applications already in the early 1970’s [1]. When TiO_2 is exposed to UV light, holes (h^+), hydroxyl radicals (OH^-), electrons and superoxide ions (O_2^-) are formed which result in oxidation reactions and decomposition of organic compounds. The photocatalytic reactions on

TiO_2-containing substrates make the surface superhydrophilic which facilitates water to wet the surface and to remove the remaining dirt residuals from it. This dual effect of TiO_2 has been utilised nowadays especially in glass, tile and steel products for construction applications [2, 3]. Different coating techniques such as sol-gel and ALD (Atomic Layer Deposition) enable incorporation of photocatalytic titanium dioxide on the surface without isolating the photocatalytic compounds from the light by a thick coating matrix. These both techniques enable manufacturing of coatings with thicknesses ranging from nanometer scale to a few micrometers.

In the sol-gel technique, a nanoscale network is typically formed from metal alkoxides through hydrolysis and condensation reactions. The process starts from a continuous liquid phase, continues with formation of colloidal suspension and leads to gelation of the sol. By tailoring and optimisation of the composition of the sol, coatings with different functional properties can be created. Enhancement of dirt repellence together with cleanability can be achieved by adequate hydrophobic and oleophobic surface properties of the coatings. Scratch resistance can be improved by incorporation of ceramic components in to the formula and flexibility is achieved with polymeric moieties. One of the many advantages of these coatings is the low viscosity providing easy applicabilty by different coating methods. In addition, the thin coatings can be transparent and maintain thereby the original appearance and often also the original feel of the substrate [4, 5].

The ALD process is based on the sequential use of self-terminating gas-solid reactions by depositing one atomic layer during one cycle in a reactor. ALD processes are exploited for manufacturing of different types of solid inorganic materials and uniform coatings for complex shape products. Oxides are the most prominent inorganic materials grown by ALD techniques. The technique enables precise control of the thickness and composition of the coatings. A great deal of studies on ALD-deposited TiO_2 on glass or mineral particles have been published, whereas clearly less published data on ALD-based TiO_2 coatings exist [6, 7, 8].

In this study, influence of the ALD and sol-gel TiO_2 coatings on surface properties such as visual appearance, wettability and topography of stainless steel (EN 1.4301) were evaluated. In addition, the photo-induced hydrophilicity of the coatings was determined and preliminary cleanability trials were conducted.

Experimental

Materials

In this study, surface treatments using sol-gel and ALD techniques on austenitic stainless steel EN 1.4301 (AISI 304) substrates with dry-brushed surface finish (2J) were investigated. The substrate surfaces were subjected to pre-treatments prior to the coating procedures with the sol-gels in order to ensure the very best adhesion properties of the coatings with the steel substrates. The surface pre-treatment included degreasing (commercial alkaline, 25°C, 5min), and rinsing (H_2O).

After the pre-treatment, the stainless steel substrates were coated with sol-gel-based nanocoatings. The basic coating developed at VTT was the low surface energy hybrid coating PSG21. This basic formula was modified with TiO_2 additions in 5 and 10 % quantities (wt-% of sol). The types of TiO_2 were commercially available ANX PA- or PS- powders manufactured and provided by Kemira Pigments Oy. The criteria taken into account in the development of the PSG21 coatings were good oil and water repellence properties with intent to promote the performance by self-cleaning functionality due to photocatalytic TiO_2. Other criteria followed in the development work were anti-fouling, abrasion, corrosion, chemical resistance and also environmental friendliness. Samples of 50 x 100 mm were spill-coated and after the application of the sol, conventional heat treatment was used to evaporate the solvents and to cure the coatings. The heat treatment took place at 110ºC for 60 min.

ALD TiO_2 coatings were deposited on the stainless steel substrates by using the temperature of 245°C. Titanium precursor was $TiCl_4$, and H_2O acted as an oxygen source. The coating thicknesses varied from 0 to 200 nm, and the coating thickness was determined from the number of the subsequent coating cycles. The growth rate of the coatings was 0.05 nm/cycle.

Methods

UV exposure of the coatings

The UV-activity of the TiO_2-doped sol-gel and ALD coatings was evaluated by comparing water repellence properties of the coated surfaces as unexposed and as exposed to UV light. The samples were exposed to a UV source with a wavelength peak at 365 nm. The distance of the samples from the UV light source was adjusted so that the light intensity on the sample surfaces was 3 mW/cm^2. The irradiation times were from 0.5 hours up to 2 days (if necessary) and the UV exposure took place in a climate room (50% relative humidity, 20^{o}C). The contact angle measurements were conducted immediately after each UV irradiation period.

Contact angle measurements

The effect of the coatings on the wettability (with water and oleic acid) of stainless steel, and on the other hand, the effect of UV exposure on the water repellence properties of the coatings were determined by measuring contact angles of static water (distilled) droplets (7 µl) on the surfaces. The instrument used for the measurements was a CAM200 videotaping system (KSV Instruments Ltd). For the contact angle calculations, the Young–Laplace equation was used. Two parallel measurements with each test substrate were carried out.

Gloss values

The effect of the coatings on the gloss values of the stainless steel substrate was evaluated by measuring spatial gloss with the geometry of 85° using an Elcometer Micro-TRI-Gloss meter.

Topography measurements

Surface topography of the non-coated and the coated stainless steel samples were monitored by means of an optical profiler (Sensofar Plµ 23000). A typical surface area of 0.25 x 0.19 mm^2 (50x magnification optics) was imaged and from each image, five line profiles were recorded for calculation of mean Ra roughness values.

Assessment of easy-to-clean properties

The effect of the sol-gel coatings developed on the anti-fouling properties of stainless steel was assessed by means of a FTIR-mapping system (Fourier Transform Infra Red Spectroscopy). Oleic acid droplets (0.5 µl) were pressed on to the test surfaces and wiped off then with a dry micro fibre cloth. The cleaned surfaces were subjected to FTIR-mapping by directing the IR-beam to the sample surfaces through microscope optics and gathering spectra of an area of 50x50 µm^2 as a map. The differences in the intensities of the spectral bands related to oleic acid are registered as different shades of color on the map. Comparison of the oleic acid coverage on the non-coated and coated surfaces after cleaning reveals the anti-fouling efficacy of the coatings.

Results and discussion

The sol-gel coating PSG21 showed excellent repellence properties when applied on the dry-brushed stainless steel substrate (Figure 1). As a result of the pre-treatments, the wettability of the substrate was improved and, thereby, the applicability/adhesion of the sol-gel coating to the substrate was expected to improve. Oily contaminants were also easy to clean from the PSG21 coating surface (as is shown later in Figure 5), and the coating was, therefore, considered as a good candidate for further modification with TiO_2.

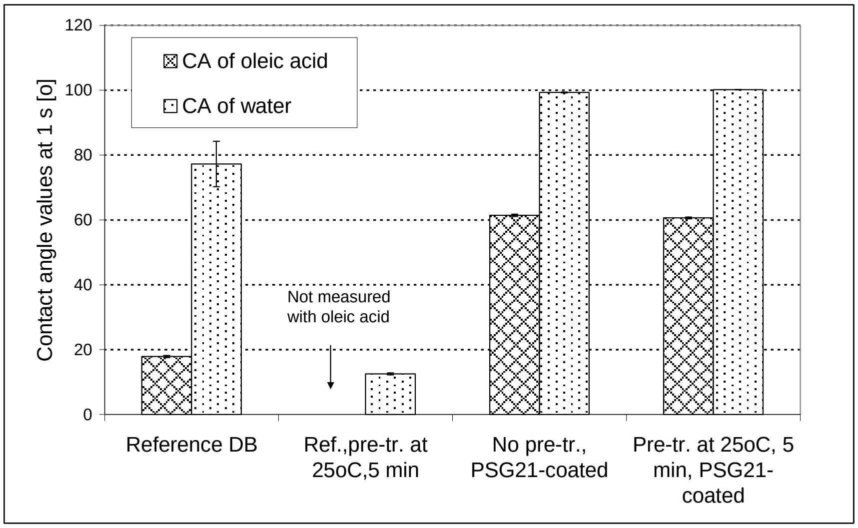

Figure 1. Effect of solvent pre-treatment on the wettability of stainless steel (EN 1.4301) and effect of the sol-gel coating PSG21 on the repellence properties of the substrate.

The thin sol-gel coating hardly changed the appearance of the stainless steel substrate, whereas TiO_2 additions (in 5 and 10%) clearly decreased the transparency of the coating. Figure 2 shows the appearance of the sol-gel coating PSG21 with and without TiO_2 compared to the non-coated stainless steel surface. The gloss values of the stainless steel substrate changed only slightly when coated with the sol-gel PSG21, whereas addition of TiO_2 resulted in clear decrease in the gloss values. The gloss values of the stainless steel substrate were practically not affected by the ALD coatings, however the ALD treatments changed the colour of the substrate. Depending on the ALD coating thickness, the shades of the coatings on the steel substrates varied in all colours of the spectra (from green to purple).

Figure 2. EN 1.4301 2J stainless steel plates as non-coated, coated with PSG21 and coated with TiO_2-doped PSG21. The spatial gloss value measured for the surfaces were around 110, 100 and 10, respectively.

Besides the chemical composition, topographical features play a significant role in the dirt resistance of a surface. As is expected from the gloss values and appearance of the TiO_2-doped sol-gels, the topography of the sol-gel coating clearly changes due the TiO_2 addition (Figure 3).

The ALD coatings had hardly any effect on the topography and roughness values of the stainless steel substrate.

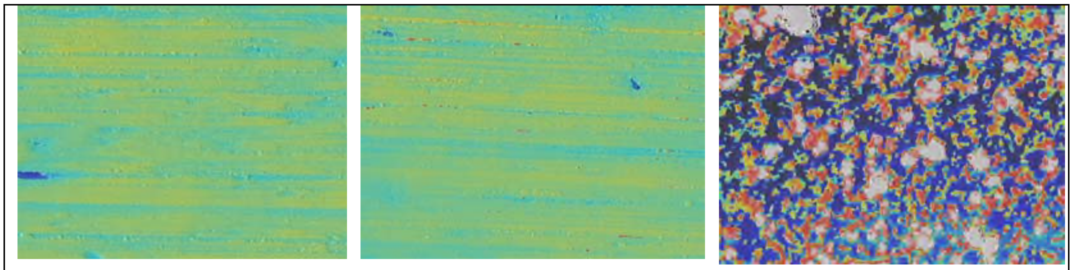
Non-coated 2J PSG21 5 % PA added

Figure 3. Area of 255 x 191 µm^2 imaged with an optical profiler from the non-coated, PSG21-coated and TiO_2 PSG21 –coated stainless steel (2J) surfaces.

Figure 4 shows the UV-induced hydrophilicity of the sol gel PSG21 coatings doped with TiO_2. The initial contact angle values (no UV exposure) revealed that the TiO_2 additions have slightly decreased the water repellence of the sol-gel (comparison with Figure 1). UV irradiation of PSG21 coating with TiO_2 did not induce any decrease in the water contact angles when exposure times less than 24 hours were used. When the exposure time was prolonged up to 48 hours, the PSG21 coating with 10 % PS type TiO_2 turned almost superhydrophilic. However, hardly any decrease in the water contact angles of the PSG21 coatings with 5 % TiO_2 additions (PA or PS) was obtained.

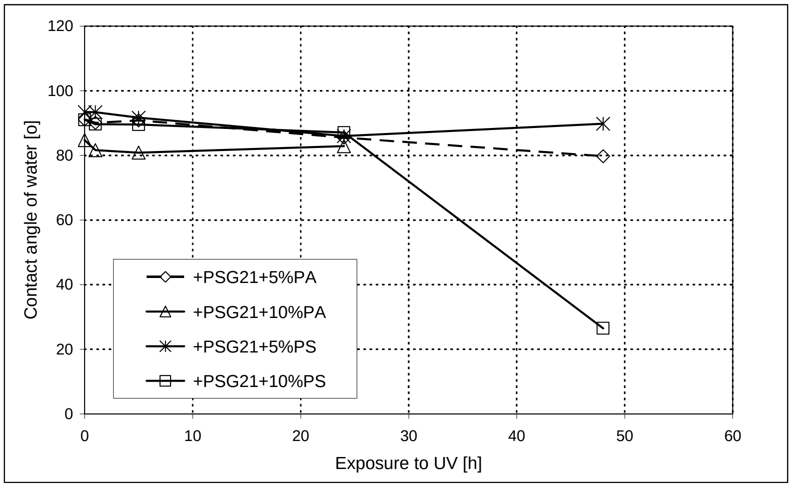

Figure 4. Contact angle of water as a function of UV exposure on TiO_2 PSG21-coated stainless steel EN 1.4301 2J. There was no data for the sol gel coating with 10% PA as exposured to 48 hours.

The ALD coatings improved to some extent the water repellence properties of the substrate: for non-coated 2J surface, contact angles less than 80° and for ALD-coated surfaces values around 81-92° were recorded. The ALD TiO_2 coatings on the 2J-finished stainless steel substrate turned highly hydrophilic already after 30 min of UV exposure. The contact angles of water dropped from around 81-92° to less than 20° irrespective of the coating thickness (Table 1).

Table 1. Effect of UV exposure on water contact angles on ALD TiO_2 –coated stainless steel (AISI 304).

Coating on 2J finish	**Contact angle of water [o]**	
	Without UV exposure	**After 30 min of UV**
ALD, 50 nm thick	91.8	14.3
ALD, 100 nm thick	88.1	12.3
ALD, 150 nm thick	85.7	6.5
ALD, 200 nm thick	80.5	7.5

For preliminary cleanability evaluation of the sol-gel coatings, the coating surfaces were stained with oleic acid (oily substance) and the residual oil was analysed by the FTIR method. The results revealed that the sol-gel coating with and without TiO_2 (5%) were cleaner than the non-coated reference after wiping of the oil stain with a micro fibre cloth (Figure 5). The remaining oil on the TiO_2 sol-gel was further removed by the UV irradiation (48 h).

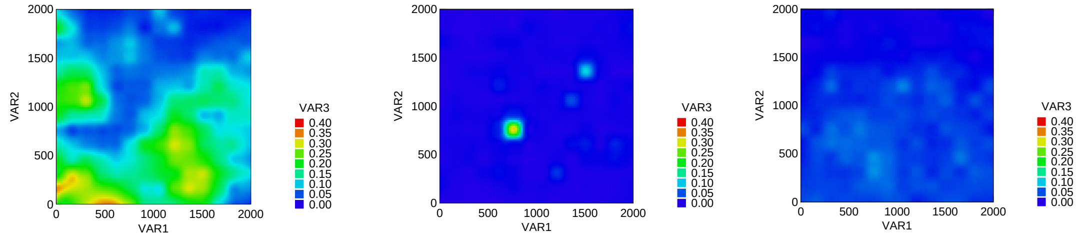

Non-coated 2J substrate with PSG21 coating with PSG21 TiO_2 (5% PA) sol-gel

Figure 5. FTIR maps of EN 1.4301 2J surfaces without a coating, with the PSG21 coating and with the sol-gel TiO_2 coating after cleaning of the oil stain from the surfaces with as micro fibre cloth.

Conclusions

The sol-gel coating developed showed its potential as an easy-to-clean treatment for stainless steel. The ALD TiO_2 coatings, especially, showed strong photoinduced hydrophilicity, and can therefore be considered as good candidates for improvement of self-cleaning properties of stainless steel. However, further development of the treatment processes and sol-gel coating formulas such as better dispersion of TiO_2 particles for enhanced performance and efficiency is needed. Particularly, the performance tests in outdoor use (some ongoing) will provide valuable information for the development of these coatings.

Acknowledgements

The study has been carried out within the Clean and Environmentally Friendly Metal Products – PUHTEET - project which has been financed by Finnish metal industry, Finnish Funding Agency for Technology and Innovation (TEKES) and VTT Technical Research Centre of Finland. Special thanks belong to Planar Inc. for manufacturing of the ALD coatings and to Outokumpu Stainless Oy and Kemira Pigments Oy for supplying the materials.

References

[1] A. Fujishima, K. Honda, “Electrochemical photolysis of water at a semiconductor electrode”, Nature 238, 1972
[2] T. Watanabe, A. Nakajima, R. Wang, M. Minabe, S. Koizumi, A. Fujishima, K. Hashimoto, “Photocatalytic activity and photoinduced hydrophilicity of titanium dioxide coated glass”, Thin Solid Films 351, 1999, pp. 260-263

[3] A. N. Khramov, N. N. Voevodin, V. N. Balbyshev, R. A. Mantz, “Sol-Gel-Derived Corrosion-Protective Coatings with Controllable Release of Incorporated Organic Corrosion Inhibitors”, Thin Solid Films 483, 2005, 191

[4] E. Miorin, C. Pagura, M. Battagliarin, M. Fabrizio, M. Guglielmi, P. Miselli, “Stain-resistant sol-gel silica coatings on stoneware tile”, American Ceramic Society Bulletin, 82, 3, 2003

[5] C. Li, K. Jordens, G. L. Wilkes, “Abrasion-Resistant Coatings for Plastic and Soft Metallic Substrates by Sol-Gel Reactions of a Triethoxysilylated Diethylenetriamine and Tetramethoxysilane”, Wear 242, 2000, pp.152-159

[6] M. Leskelä, M. Ritala, "Atomic layer deposition (ALD): from precursors to thin film structures", Thin Solid Films, 409, 2002, pp. 138-146

[7] R. L. Puurunen, “Surface chemistry of atomic layer deposition: A case study for the trimethylaluminium/water process”, Journal of Applied Physics; Applied Physics Reviews, 97, 2005, pp.121301:1 – 50

[8] H. Kawakami, R. Ilola, L. Straka, S. Papula, J. Romu, H. Hänninen, R. Mahlberg, and M. Heikkilä. "Photocatalytic Activity of Atomic Layer Deposited TiO_2 Coatings on Austenitic Stainless Steels and Copper Alloys", Journal of the Electrochemical Society, 155 (2), 2008, pp. C62-C68

CORROSION RESISTANCE OF TIN PVD INTERMETALLIC COATINGS ON 316L STAINLESS STEEL IN 3.5% AND 12% NaCl SOLUTION AT 25˚C AND 70˚C

E. Viyanit[1], S. Ouampan[2], P. Khumsuk[1], K. Wongpinkeaw[1]

[1]National Metal and Materials Technology Center (MTEC), Thailand, [2]Suranaree University of Technology (SUT), Thailand

Abstract

In pharmaceutical industry, many engineering components made of 316L stainless steel are prone to early failure caused by environment-induced corrosion (EIC). Therefore, increasing the corrosion resistance of 316L stainless steel exposed to the given service conditions was aimed in the present contribution. The arc plama assited physical vapour deposition (PVD) was used to produce TiN intermetallic coatings with a thickness of approximately 2 microns. In order to study the effects of TiN intermetallic coatings on the corrosion resistance improvement of stainless steel substrate, the potentiodynamic polarization measurements in 3.5% and 12% NaCl solutions at 25˚C and 70˚C were conducted. Additionally, the morphology and structure of TiN intermetallic coatings was analyzed by using scanning electron microscopy (SEM) and X-ray diffraction.

The results from the potentiodynamic polarization measurements revealed that the corrosion potentials were not much different for the TiN-coated sample with respect to the uncoated one, whereas the breakdown potentials of the TiN-coated samples were obviously higher than that of the uncoated ones. However, the breakdown potentials were decreased with increasing either temperature or NaCl concentration in the testing solution, or both. Moreover, the TiN-coated sample showed the passive current density, approximately one order of magnitude lower compared with the uncoated one, and particularly at 25°C.

Introduction

316L austenitic stainless steel is very attractive for many industrial applications, i.e. oil & gas production, petrochemical, pharmaceutical industries, etc., due to its relatively high corrosion resistance to corrosion in comparison to 304L stainless steel.[1,2] In addition, it has suitable mechanical properties, good fabricability and weldability. However, localized corrosion, e.g. pitting corrosion, is a major concern for the application of 316L stainless steel in the environment with the presence of halide ions, in particular the chloride ion.[3-5]

In previous reports [6-8], the fretting corrosion resistance of TiN-PVD coating on stainless steels was studied in the solutions with various concentration of sodium chloride. It is evident that the TiN-PVD coating greatly improved the corrosion resistance of stainless steel compared with uncoated one. On the other hand, the presence of permeable defects, e.g. pores and pinholes, which provide direct paths for corrosive electrolyte to reach the substrate, caused a drastic decrease in corrosion resistance with the formation of seriously localized corrosion [9]. Therefore, the quality of coating must be taken into account in the PVD process control to ensure the increasing lifetime of the TiN-PVD coated stainless steel.

Based on the engineering approach of materials selection in the pharmaceutical industry, 316L stainless steel is regarded as a basic material for any components exposed to corrosive environments in service. However, this kind of stainless steel is prone to corrosion resulting in early failure of the components when more aggressive solutions such as the 12%-NaCl surfactant are being used in the process. Moreover, increasing the service temperature is a important factor to decrease the corrosion resistance of austenitic stainless steels with showing a linear decrease in pitting potentials. The gradient of the pitting potential decrease was approximately -3.3 mV/˚C for 304, 316 and 904L stainless steels in the temperature range of 20 and 90˚C[10]. Thus, any techniques of surface modification might be used to enhance corrosion resistance of critical components instead of replacement with more expensive corrosion resistant alloys.

In order to study the possibility of applying the TiN-PVD coating technique to the critical components regardless of replacement with more expensive corrosion resistant alloys in the pharmaceutical industry, the present contribution aimed at gaining a meaningful understanding on the corrosion behavior of TiN-coated 316L stainless steel prepared by a commercial PVD system in the 3.5% and 12% NaCl solutions at temperatures of 25˚C and 70˚C by means of potentiodynamic polarization measurements.

Materials and experimental method

Materials and specimen preparation

The rectangle specimens with the dimensions 30mm×30mm were cut from 316L stainless steel having thickness of 2mm. The chemical composition of the steel was given in Table 1. In order to prepare the samples as references for corrosion tests and as substrates for PVD coatings, the specimens were ground up to 1000-grit SiC paper on the one site, degreased with acetone, dried with hot pressurized air, and kept in a desiccator until use. TiN-coated samples were obtained by cathodic arc plasma deposition in a commercial PVD reactor at Nanoshield & Royal Ace, Thailand. Before the coating process, the samples were thoroughly degreased and ultrasonically cleaned in an acetone bath. The TiN coatings were deposited at temperature of approximately 300°C with given PVD atmosphere, pressure, bias and deposition time to obtain a specified coating thickness.

Table 1. Chemical composition of 316L stainless steel

Element	C	Cr	Ni	Mo	Mn	Si	P	S	Fe
(wt.%)	0.031	17.03	12.01	2.48	2.00	1.00	0.045	0.03	Bal.

Coating examination

The microstructure and coating thickness of the TiN-coated samples were examined by using optical (OM) and scanning electron microscopy (SEM). Additionally, the X-ray diffraction (XRD) technique was undertaken to identify the phases present in the coating layer.

Corrosion test

The potentiodynamic polarization measurements were conducted in accordance with ASTM standard G5 by using a typical 3-electrode corrosion cell linked with a AUTOLAB PGSTAT 30 potentiostat/galvanostat in order to study corrosion behavior of the TiN-coated stainless steel compared with the uncoated one as shown in Fig. 1. Copper wire was connected to the samples opposite to the testing site, which is necessary for an electrical circuit connection to the potentiostat. Subsequently, lacquer was manually applied on the surfaces of the samples and copper wire to specify only the testing area of 1 cm^2 exposed to the testing solution with eliminating the uncontrolled parameters from non-measurable areas. During the corrosion test, the sample was immersed in the naturally-aerated 3.5% and 12% NaCl solutions at the controlled temperatures of 25 and 70˚C, respectively. After a 30-min exposure to the test solution, the potential scan was started at 100 mV below the open-circuit potential versus a Ag/AgCl electrode with a sweep rate of 0.5 mV/s. As the breakdown potential appeared, the potential scan was stopped when the current density of 1.0E-02 A/cm^2 was reached, so that the resistance to localized corrosion in terms of the breakdown potential was evaluated. After polarization measurements, the morphology of pits occurring on the surface was examined by optical microscopy (OM) and scanning electron microscopy (SEM).

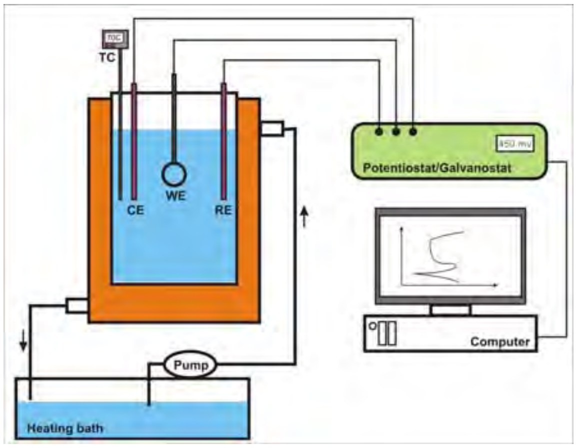

Figure 1. Schematic instrumental setup for potentiodynamic polarization measurements.

Results and discussion

Coating examination

As shown in Fig. 2, the gold-like color surface is obtained for the TiN-coated stainless steel by the PVD technique in comparison to the silver color of the uncoated sample. Fig. 3 reveals a TiN coating with approximately 2 μm thickness on the substrate, but that thickness is still variable due to the adjustment the PVD parameters, e.g. substrate bias, anode-cathode distance, etc. It is meaningful for engineers to define the dimensional tolerance for precision components to be undergone the surface treatment by the PVD technique. Fig. 4 shows the XRD patterns of the TiN coating, in which the position of TiN peaks indicates that the film is stoichiometric[12] and has the phase structure as osbornite. Therefore, the XRD results verify the formation of the TiN layer on the stainless steel.

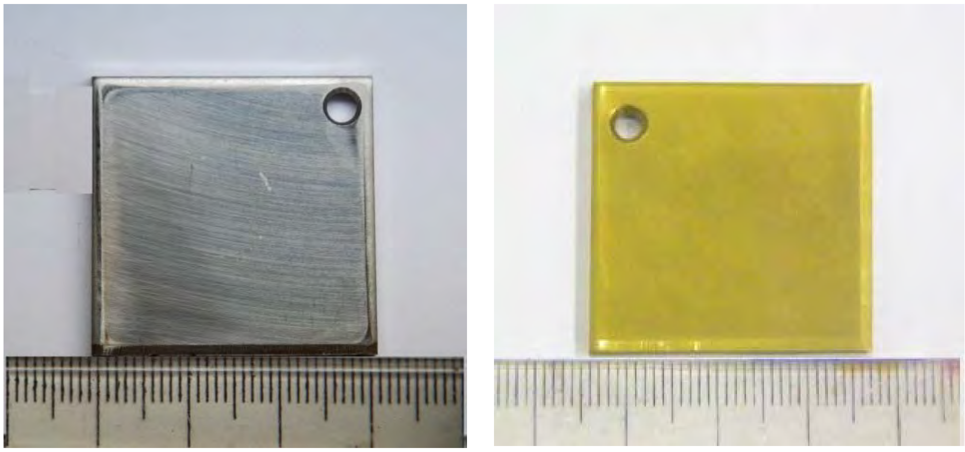

a) Stainless steel substrate

b) TiN coated stainless steel

Figure 2. Physical appearances of stainless steel substrate and TiN-coated stainless steel.

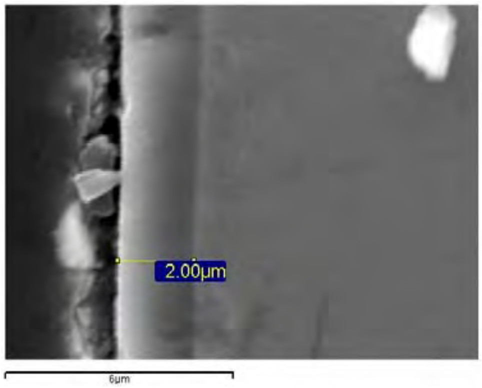

Figure 3. SEM micrograph of a cross-sectioned TiN film on 316L stainless steel substrate.

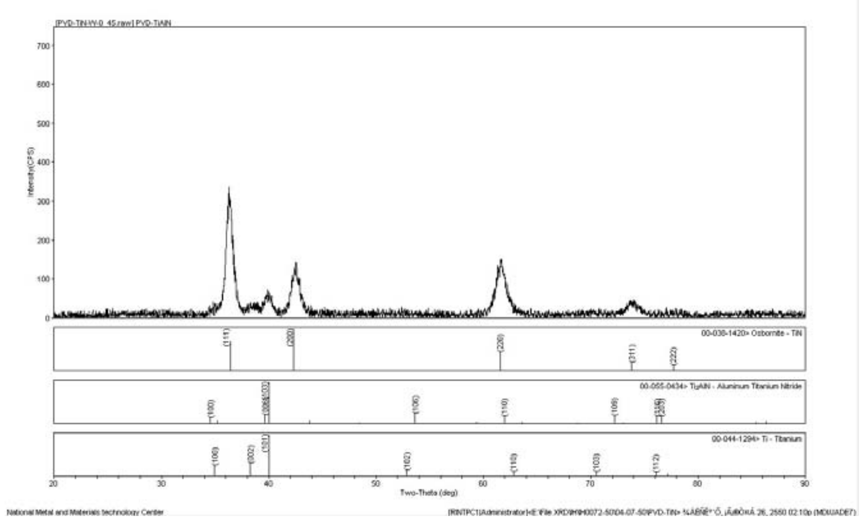

Figure 4. The XRD pattern of TiN-coated stainless steel.

Corrosion tests

The polarization curves of the TiN-coated stainless steel in the 3.5% and 12% NaCl solutions at 25˚C were recorded as shown in Fig. 5. It can be seen that the breakdown potential of the TiN-coated sample, 1220 mV (Ag/AgCl), is much higher than that of the uncoated one, 360 mV

(Ag/AgCl), when tested in the 3.5% NaCl solution. However, the breakdown potentials of both samples were decreased to half as the 12% NaCl solution was used. Again, it must be noted that the polarization curves of the TiN-coated samples revealed the passive current density of about an order of magnitude lower relatively than those of the uncoated ones. Additionally, the TiN coating showed its increased passive potential range with respect to the uncoated one. However, the passive potential range was decreased by increased NaCl concentration in the solution. These phenomena should be attributed to the increased chloride ions resulting in promotion of localized corrosion. Breakdown potential and passive potential range of uncoated and TiN coated stainless steels in 3.5% and 12% NaCl solution at 25°C are given in Table 2.

As testing temperature increased to 70°C, the TiN-coated and uncoated samples still maintained their passive behavior. However, the breakdown potentials were drastically decreased from 1220 mV (Ag/AgCl) to 578 mV (Ag/AgCl) for the TiN-coated samples and from 360 mV (Ag/AgCl) to 190 mV (Ag/AgCl) for the uncoated one as tested in the 3.5% NaCl solution. Decreasing the breakdown potentials also caused a decrease in the passive potential range, as shown in Fig. 6a. In case of testing in the 12% NaCl solution, the TiN coating cannot provide the corrosion resistance significantly different from that of the uncoated stainless steel, as shown in Fig. 6b. The breakdown potentials below 150 mV (Ag/AgCl) with the shortened passive potential ranges also showed. Therefore, the TiN coatings by the PVD technique should not be suitable for improvement of corrosion resistance if the component must be exposed to the aggressive environment, e.g. 12% NaCl solution at temperature above 70°C. Table 3 lists the breakdown potentials and the passive potential ranges obtained by evaluating the polarization curves of the TiN-coated and uncoated samples in the 3.5% and 12% NaCl solution at 70°C.

In general, the breakdown potential is normally used to explain the corrosion resistance of alloys having passive film so that the various characteristics of pit formation account for changing such a breakdown potential. As shown in Fig. 8, the larger pits appear preferably on the surface of the uncoated sample due to less noble oxide film compared with the TiN coating.

Although the key role of chloride in the pit formation is still not understood clearly, some physical models have been proposed to explain the effects of chloride on the pit nucleation and propagation[11]. It is well known that the resistance to localized corrosion of stainless steel is correlated to the characteristic of the passive film, which is markedly impaired by chloride ions[12]. These chloride ions derived from the chloride-containing solutions attack the passive or protective film with a consequence of the pit nucleation and propagation, when such chloride ions reach the metal matrix[13,14]. Therefore, increasing the NaCl concentration in the testing solution means the increased chloride ions resulting in acceleration of the pit nucleation rate with showing the lower breakdown potential on the polarization curve.

As described in the previous contribution[10], the breakdown potentials of austenitic stainless steels were linearly decreased with increasing temperature. Due to the fact that corrosion is an electrochemical reaction influenced by temperature, increasing temperature leads to a decrease in the passive potential range connected with the decreased breakdown potential. On the other hand, the passive current density is increased by increasing temperature[15]. These explanations agree very well with the results obtained in the present study.

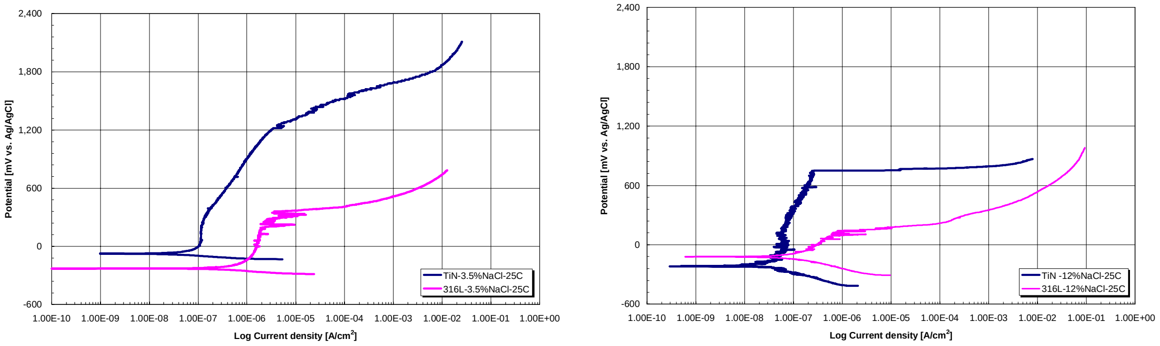

a) 3.5% NaCl solution b) 12% NaCl solution

Figure 6. Polarization curves of TiN coated and untreated 316L stainless steel in 3.5% NaCl solution at 25˚C.

Table 2. Breakdown potential and passive potential range of uncoated and TiN coated stainless steels in 3.5% and 12% NaCl solution at 25˚C.

NaCl Concentration (wt.%)	Breakdown potential (mV)		Passive potential range (mV)	
	Uncoated	TiN coated	Uncoated	TiN coated
3.5	360	1220	588	1295
12	144	749	264	969

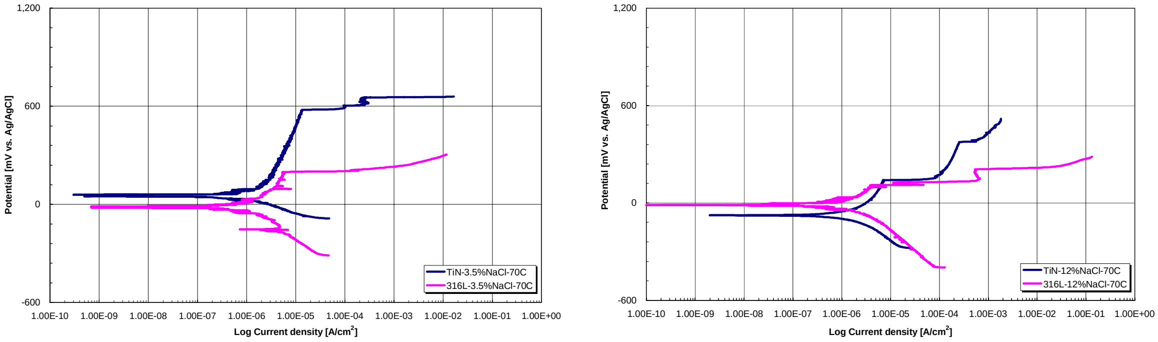

a) 3.5% NaCl solution b) 12% NaCl solution

Figure 7**.** Polarization curves of TiN coated and untreated 316L stainless steel in 12% NaCl solution at 70˚C.

Table 3. Breakdown potential and passive potential range of uncoated and TiN coated stainless steels in 3.5% and 12% NaCl solution at 70˚C.

NaCl Concentration (wt.%)	Pitting potential (mV)		Passive potential range (mV)	
	Uncoated	TiN coated	Uncoated	TiN coated
3.5	198	578	211	520
12	110	140	124	213

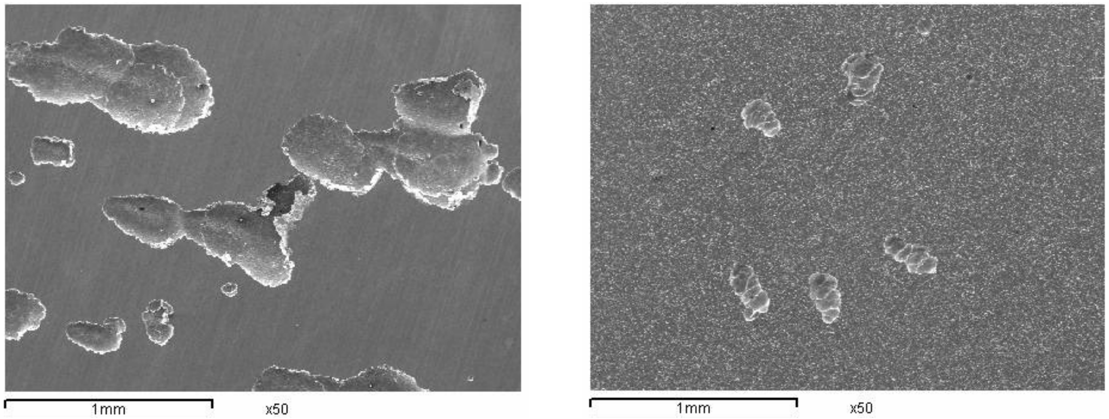

a) Uncoated specimen b) TiN coated specimen

Figure 8. SEM micrographs of the uncoated and TiN coated 316L stainless steel with the presence of pits after potentiodynamic testing in the 12% NaCl solution at 25˚C.

Comparing the effects of increased chloride ions and temperature on the corrosion resistance, the TiN coatings indicate the remarkable resistance to corrosion, in particular, when exposed to the 3.5% NaCl solution. In contrast, protective properties of the TiN coatings were significantly impaired when the 12% NaCl solution and temperature of 70°C were consider as the most aggressive for the present study. However, further studies are going to be conducted to get a better understanding of the improvement of corrosion resistance by the TiN-PVD coating film.

Conclusions

From the present study on corrosion behavior of the TiN-coated and uncoated 316L stainless steels, the following conclusions can be drawn:

- TiN coatings on stainless steel were successfully done by the PVD technique to enhance the corrosion resistance of the substrate.
- At room temperature, 25°C, the TiN coatings were as protective, whereas the uncoated stainless steel lost significantly its protective properties when the 12%NaCl solution was used.
- TiN coatings were not sufficient to enhance the corrosion resistance in the instance of the most aggressive condition, 12%NaCl solution at 70°C, as was expected.
- Increased temperature and NaCl concentration were the important parameters to control the corrosion resistance in terms of the breakdown potential and passive potential range of the TiN-coated and uncoated stainless steels.
- Based on technical-economic aspects of implementation of the PVD technique to any components in the corrosion applications, further studies should be performed to provide useful information to industries.

References

[1] A. Turnbull et al., Corrosion Science 45 (2003), pp. 1051–1072
[2] A. Turnbull and S. Zhou, Corrosion Science 46 (2004), pp. 1239–1264
[3] K. Zhang et al., Surface & Coatings Technology 201 (2006), pp. 1393–1400
[4] G.H. Koch, MTI Publication No. 41, Materials Technology Institute of the Chemical Process Industries, Inc., Published for MTI by NACE Int., Houston TX, 1995
[5] D. Bauernfeind and G. Mori, Corrosion2003, NACE International, Houston TX, Paper No. 03257

[6] D. Lopez, C. Sanchez and A. Toro, Wear 258 (2005), pp.684–692
[7] C. Liu, A. Leyland, S. Lyon and A. Matthews, “Surface and Coatings Technology” 76-77 (1995), pp. 615-622
[8] S. Rossi, et al., Thin Solid Films 350 (1999), pp.161-167
[9] C. Liu, Q. Bi, A. Leyland and A. Matthews, Corrosion Science 45 (2003), pp.1243–1256
[10] N.J. Laycock and R.C. Newman, Corrosion Science 39, 1997, pp. 1771 – 1790
[11] Z. Szklarska-Smialowska, Corrosion Science 44 (2002), pp. 1143-1149
[12] J.M. Bastidas, C.L. Torres, E. Cano and J.L. Polo, Corrosion Science 2002, p625-633
[13] H.-P. Feng et al., Materials Science and Engineering A347, 2003, pp. 123-129
[14] A.H. Faraji, Corrosion 2002, Paper No. 02439, NACE International, Houston, TX, 2002
[15] D.A. Jones, “Principle and Prevention of Corrosion”, 2nd Edition, Prentice Hall International, Singapore, 1997.

CHARACTERIZATION AND OPTIMIZATION OF THE FUNCTIONAL PROPERTIES OF STAINLESS STEEL SURFACES

T.L. Ladwein, M. Sorg, S. Schilling

Aalen University of Applied Sciences, Germany

Abstract

Chemical resistance of stainless steel components is due to their their functional surfaces that are responsible for the corrosion resistance and also for other properties such as the adhesion of substrates or cleanability. The passive layer forms the phase boundary between the metal and environment. It is formed either spontaneously during the fabrication or it can be produced in an accelerated way by specific chemical treatments. The quality of the passive film is dependant on the alloying content of the metal, but also influenced by other factors such as fabrication process, surface topography and type of mechanical and chemical surface treatment. The passive layer is also a kind of living system whose properties and stability is largely influenced by the environment where it is used in. So far, there are no methods to characterize these functional surface properties in a generally applicable way. Special electrochemical techniques in combination with measurements of the surface energy have shown to be a useful tool. This permits to characterize and to classify the functional properties of surfaces which have been produced by mechanical and special chemical and electrochemical treatments.

Introduction

The functional properties of materials are determined by their behaviour in contact with various substances, i.e. the corrosion and tribological behaviour as well as the adhesion of the substances to the metal. The latter behaviour is responsible for the cleaning properties of the equipment.

Various grades of stainless steels are widely used in food, CPI and pharmaceuticak industries because of their corrosion resistance and their ease in fabrication[1]. Additionally, as they can be rolled with shiny and even surfaces with low roughness they are supposed to be easy to clean. Additionally, they can be electropolished to produce non-sticky surfaces. This procedure, which is effective but also time consuming and costly, is often applied in paper machines and pharmaceutical industries[2].

Though a low roughness is often considered to be essential for the adhesion properties is has been shown that the surface preparing process is as important as the roughness. This is also valid to corrosion properties, as reported by Volmer[3] and Ladwein and Guempel[4,5].

Due to these complex interrelationships it is not trivial to characterize and quantify the functional surface properties. Measuring the roughness by mechanical or optical procedures is not good enough. Measuring of surface energies by means of wettability tests can be another alternative. Goellner et al.[6] proposed to use electrochemical noise, for this method is very sensitive to even slight variations of the surfaces and their passive layers and therefore it can help to differentiate between various types of surface structures[7,8].

Experimental

Test Materials

Test specimen were cut in sizes 20x20 mm from a cold rolled sheet (3 mm thick) of stainless steel 1.4404 (AISI 316L) in the as-delivered condition. A copper wire was spotwelded on the backside and the specimen mounted in a metallografic sample using an epoxy resin permiting a gap-free mounting. Surface preparations were applied by wet-grinding the specimen on a metallografic disc using emery papers of various grits and controlling thr force in all cases. The ground specimen were cleaned with deionized water and acetone and dried in a stream of hot air. Pickling took place at room temperature in a mixture of 4% HF and 30 % HNO_3. Pasivation was done by storing the prepared specimens in air for a given time or by immersing them into 30 % nitric acid.

Topography

The surface topography was evaluated using a laserprofilometer that permitted to draw pictures of the surface structures and also to determine roughness values.

Surface energy

Surface energies were measured by determining the contact angles of water and diiodomethane by the sessile drop method using an automatic device that records the contact angle with a video camera and permits a calculation of the polar and dispers parts of the surface energies directly.

Electrochemical experiments

Most of the electrochemical experiments were done with a microcell that permitted the evaluation of the specifically prepared surface area only. The size of the measuring spot was between 0.15 and 1 mm². The details of the experimental set-up are given elsewhere[9]. The electrochemical noise measurements were done with an analog potentiostat equiped with low-pass filter amplifers for potential and current noise with PC-interface and digital data storage and evaluation system. Electrochemical impedance measurements were made with a digital potentiostat with PC-controlled data storage and evaluation system. The current noise was recorded between one specimen and a platinizd titanium mesh counter electrode as a response to an anodic potential scan. Potentials were measured against a 3.5 m Ag/AgCl electrode.

Test solutions

Test solutions were made using p.a. grade chemicals (sodium chloride and deionized water). There was no specific pH control.

Results

Topography

The surface roughness was determined in terms of Ra values. In the ground states the roughness is dependant on the grit, even though there is not big difference between a 800 gr and a 1200 gr preparation. Polishing with an acidic polishing fluid results in a greater roughness than the only ground specimen. Polishing with a neutral fluid, however, resulted in a Ra between 0.03 and 0.05 µm without a marked difference between the pre-preparation by grinding. Pickling increased the Ra values again, whereby longer pickling times produced higher Ra values.

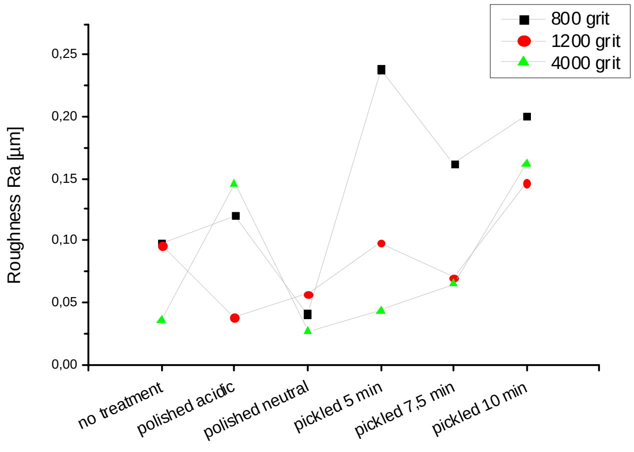

Figure 1. Surface roughness of the various preparations

Surface energy

Contrary to above, the measurements of the surface energies showed lower values for the pickled specimens compared to ground and ground and polished ones. There is not big difference between the specimens with different pickling times. Contrary to that, the polishing with an acidic fluid resulted in considerably higher surface energies for the specimens pre-ground with 800 gr and 1200 gr. Obviously pickling has a positive influence on the surface energy that is not related only to the roughness in terms of Ra-values.

Electrochemical Experiments

Thw finding concerning the surface energies was reflected in the results of the electrochemical measurements as well: polishing and pickling led to a dramatic shift of the breakthrough potentials to positive values. For the 800 gr pre-prepared surface this shift was almost 350 mV. Only for the 4000 gr pre-prepared specimen the pickling for longer times resulted in a negative shift of the breakthrough potentials. The curves taken with the microcell show a very steep rise of the current at the breakthrough potential which makes the determination of the breakthrough potential much easier than with conventional measuring techniques.

The electrochemical current noise that was recorded simultaneuosly is a very sensitive tool to identify even early activities of corrosion. It confirms the findings in the DC polarization curves. The specimen 800 gr without any further treatment showed some pre-peaks before the final breakthrough. At exactly the same potential the current noise curve confirms the activity.

Figure 2. Surface energies of the various preparations

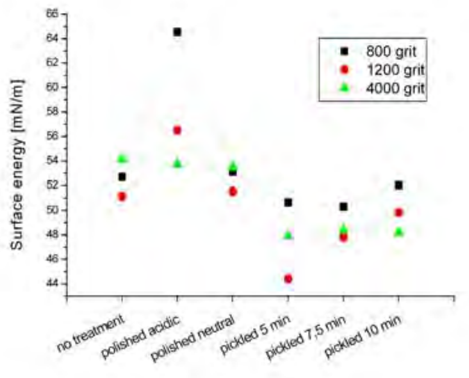

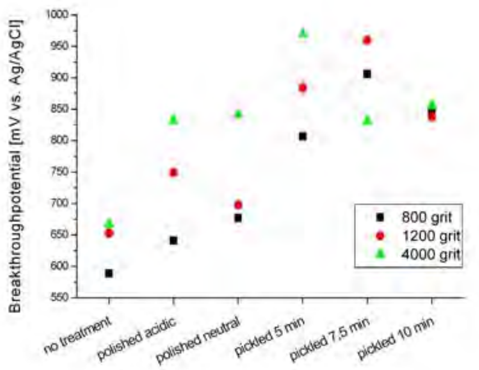

Figure 3. Breakthrough potentials in potentiodynamic scans in 3 % NaCl after various surface treatments

For the pickled specimen these pre-peaks have disappeared and the current noise gradients are only found after the breakthrough potential has been exceeded. This is different from the findings with macro-cells or immersion cells, where the noise activity is always found at much lower potentials than the breakthrough.

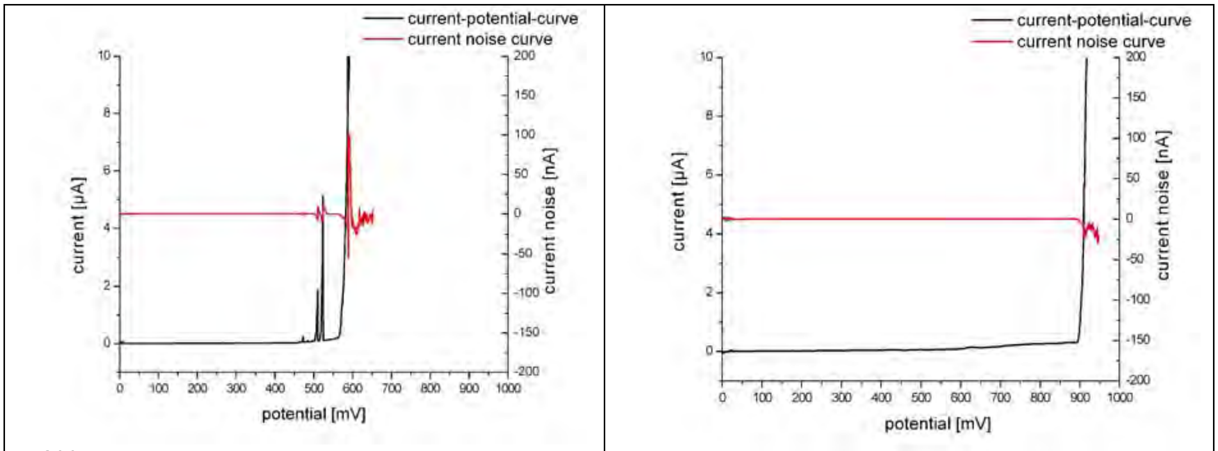

a. 800 gr

b. 800 gr + pickled 7,5 min

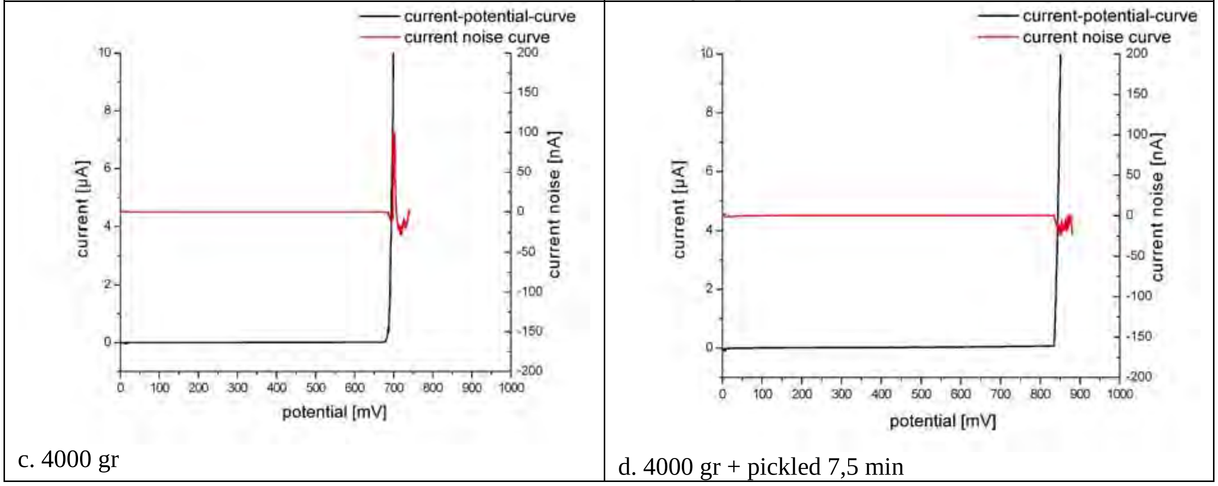

c. 4000 gr

d. 4000 gr + pickled 7,5 min

Figure 4. Polarization curves and current noise curves of various surface preparations, 3 % NaCl, room temperature

Aside of the method of surface preparation the formation of the passive film plays an important role. This could be shown by electrochemical impedance measurements which were also taken with a microcell. In the Bode plots both the impedance and phase curves show very different shape in respect to the time of passivation in air.

With increasing time the impedance increases at all frequencies, and the phase forms a characteristic negative peak at 0.1 Hz which is an indication for passive behaviour. In comparison, a 30 min passivation with nitric acid immediately after grinding does not show this characteristic peak, indicating that the behaviour in this state – chemically passivated – is obviously different from that which has been developed in air – naturally passivated. Further information is excpected after fitting the curves which is ongoing work.

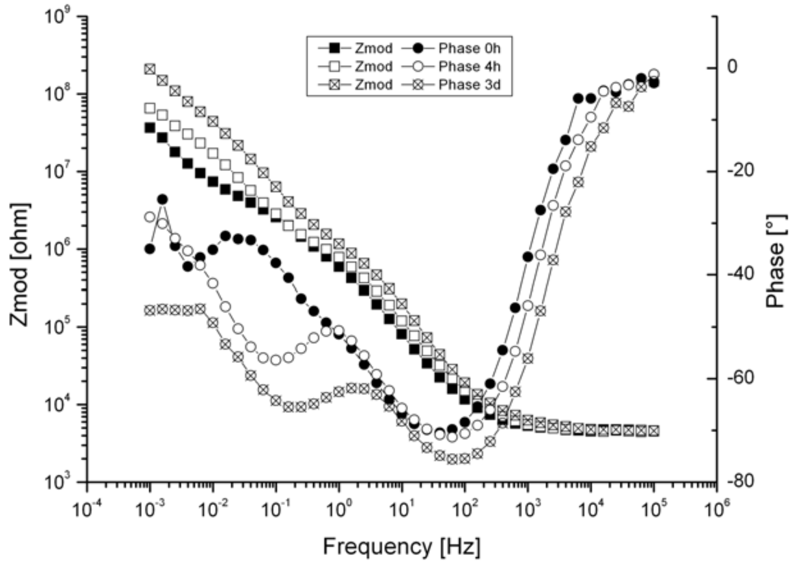

Figure 5. Electrochmical impedance spektra of fresh ground samples and passivated in air for 4 hours and 3 days respectively

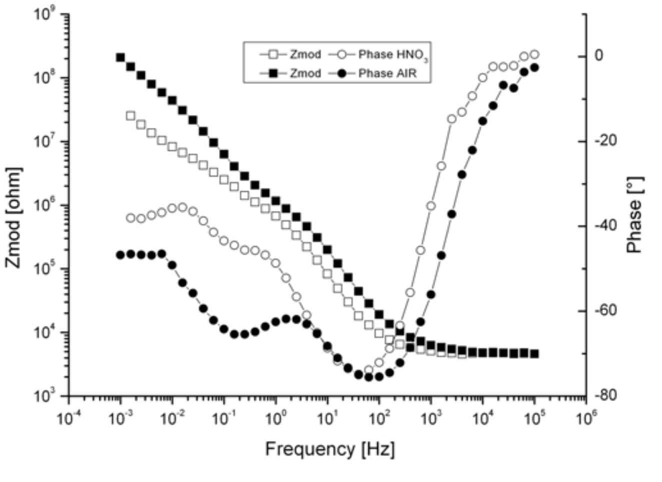

Figure 6. Electrochemical impedance spektra of specimens passivated in air and by nitric acid

Conclusions

The work indicates that the functional properties of stainless steel 1.4404 can be strongly influenced by the surface treatments. Grinding can result in very smooth surfaces with Ra-values down to 0.03 µm. Pickling these surfaces results in higher Ra-values, up to 0.2 µm. Contrary to that, however, it appeared that the surface energies of the pickled specimens are lower than those of the smoother ground surfaces, meaning that this is a more favourable situation in spite of the higher Ra-values. This is also reflected in the polarization curves and the current noise curves which show a strong correlation with the surface energy. Pickled specimens can have a breakthrough potential even 350 mV higher than that of the ground specimen.

With impedance measurements it could be shown that stable passive behaviour is developed with time. Passivation with nitric acid immediately after the grinding operation did not show the same, but the Bode plot indicates that there is obviously a difference in the passive film of the chemically passivated and naturally passivated steels.

Electrochemical microcells are shown to be a most useful tool to determine the functional surface properties permitting to take measurements on the surface under consideration without the need of special means to prepare and contact the specimen. This can also be done in a non-destructive way meaning that on-site measurements and characterization are possible.

Acknowledgements

The authors gratefully acknowledge the financial support form the German Federal Ministry of Education and Research (BMBF) under the program managing executive AiF in the frame of the program “Ingenieurnachwuchs” (Contract No. 17 N11 07).

References

[1] J. Hofmann, K. Sommer, “Hygienic design von Anlagen und deren Qualifizierungsmethoden”, Chem. Ing. Techn. 78, 1605 – 1614 (2006)
[2] U. Bobe, G. Wildbret, “Anforderungen an Werkstoffe und Werkstoffoberflächen bezüglich Reinigung und Beständigkeit”, Chem. Ing. Techn. 78, pp. 1615 – 1622 (2006)
[3] T. Vollmer, “Oberflächenbehandlungsverfahren und deren Auswirkungen auf die Korrosionsbeständigkeit von nichtrostenden Stählen”, Diploma thesis Fachhochschule Konstanz, FB Maschinenbau, Konstanz, Germany 1993
[4] T. Ladwein, P. Gümpel, “Influence of the surface texture of ferritic austenitic stainless steels on the adhesion of substrates and the corrosion resistance”, Duplex America 2000, Houston, TX, USA, 29.2. – 1.3.2000, pp. 105 - 107
[5] T. Ladwein, P. Gümpel, “The influence of Functional Properties of Stainless Steels on Corrosion”, NACE Corrosion 2004, paper 04223, NACE International, Houston, TX USA
[6] J. Goellner, “Elektrochemisches Rauschen bei der Korrosion”, Materials and Corrosion 55, 727 – 743 (2004)
[7] A. Burkert, K. Schilling, A. Heyn, “Einfluss der Schleifbehandlung auf das Korrosionsverhalten von Chrom-Nickel-Stählen”, Materials and Corrosion 55, 787 – 793, (2004)
[8] M. Bierwirth, J. Goellner, A. Heyn, “Passivation of stainless steels measured with electrochemical noise”, NACE Corrosion 2006, Paper No. 06428, NACE International, Houston, TX, USA
[9] T. Ladwein, M. Sorg, J. Maier, “Microelectrochemical techniques for characterization of the behaviour of corrosion resistant alloys”, NACE Corrosion 2008, Paper No. 08369, NACE International, Houston, TX, USA.

NANOSCALE OXIDATION OF Fe-17Cr BY OXYGEN AND WATER VAPOR: CHEMICAL COMPOSITION AND MORPHOLOGY OF THE SURFACE

P. Jussila, M. Hirsimäki, M. Koskela, K. Lahtonen, M. Lampimäki, M. Valden

Tampere University of Technology, Finland

Abstract

Nanoscale oxides (typically 1-3 nm thick) which form on stainless steel surfaces play an important role in many modern applications of these materials. In addition to their intrinsic corrosion resistance, the oxides work as the substrate for any coating material and thus affect adhesion and other interfacial properties. Recently, stainless steels have received much interest as medical materials. In such applications, the nanoscale oxides protect tissues against harmful release of metal cations (especially Ni), and their composition and morphology determine the interactions with biomolecules and biocompatible coatings. In order to further develop such properties, the formation of nanoscale oxides must be understood and controlled in detail.

In this work, the nanoscale oxidation of Fe-17Cr (EN 1.4016, AISI 430) was studied at 50 °C by photoelectron spectroscopy. This relatively simple, ferritic alloy acts as a model system for stainless steel materials and its study is intended as the first step towards more complex and functionalized surfaces. The processes of oxidation by pure molecular oxygen and water vapor are compared and their interplay in practical environments is discussed.

Inelastic electron background analysis was used to quantify the oxidation-induced changes to the chemical composition and morphology of the surface. Our results indicate the formation of an iron-rich oxide in the presence of pure O_2 and a chromium-rich oxyhydroxide in pure H_2O. The possibility to modify the surface by hydroxyl groups has significance for controlled adsorption of molecules in modern applications. The presented research methods are generic enough to be applied in any studies of such surface-mediated processes on stainless steel materials.

Introduction

Stainless steel materials are well known for their intrinsic corrosion resistance originating from a Cr-rich passive oxide which forms spontaneously on the surface under oxidizing conditions. Knowledge of the atomic-scale oxidation and segregation phenomena, however, remains rather limited despite their fundamental and technological importance. The details of these processes can be readily investigated by methods of surface science such as x-ray photoelectron spectroscopy (XPS), low energy electron diffraction (LEED), and scanning tunneling microscopy (STM).[1] These non-destructive analytical methods are sensitive to the chemical composition and structure of the outermost atomic layers in a material and thus enable studies of controlled adsorption of atoms, molecules or ions. This has contributed to the development of novel coating methods. Recent examples include fabrication of biofunctional stainless steel for bone-bonding[2] and surface modification to improve the adhesion of protective organic coatings.[3] Furthermore, there is an increasing interest towards the adsorption of proteins, which is involved in the formation of biofilms and has relevance to stainless steel materials in marine, food and biomedical industries.[4] In all these applications, the substrate oxide layer plays a crucial role.

In this work, we present an *in situ* XPS investigation of nanoscale oxide formation on a ferritic stainless steel surface upon exposure to oxygen and water vapor. Understanding and controlling this ubiquitous phenomenon forms the basis for developing novel functional properties which stem from the nanoscale surface structure.

Experimental

The investigated polycrystalline ferritic Fe-17Cr stainless steel (EN 1.4016, AISI 430) was manufactured by Outokumpu Stainless Oy (Tornio, Finland). The composition of the bulk alloy is 81.8 at.% Fe, 17.3 at.% Cr, 0.5 at.% Si, 0.2 at.% Ni, 0.2 at.% C, 0.03 at.% Mn, and 0.002 at.% S. Sample disks (9 mm diameter) were cut from cold rolled, bright annealed sheets, chemically polished, and rinsed with ethanol prior to loading into the ultra high vacuum (UHV) surface analysis system, which has been described in detail elsewhere.[5] Base pressure during the experiments was of the order of 1×10^{-10} mbar.

The sample surface was prepared *in situ* by cycles of 2.0 keV argon ion sputtering and subsequent annealing to 400°C for 10 min to remove sputter-induced defects. It was allowed to cool down slowly (within 1 h) to 50°C before the oxidation experiments.

Oxygen exposures were performed by backfilling the UHV chamber with 1.3×10^{-8} to 2.7×10^{-6} mbar of O_2 (99.9999 % purity) while maintaining the sample temperature at 50°C. The low oxygen pressure was used to kinetically control the oxidation rate so that the process could be observed in stages. The investigated range of oxygen exposures was 0 to 10^4 Langmuirs (1 L = 1.3×10^{-6} mbar s).

Reactions between the surface and water vapor were carried out in a microchamber designed for high pressure gas exposures. A Pyrex glass vial containing deionized water was connected to the chamber via a bellows-sealed valve. Dissolved gases present in the liquid were first removed by several freeze-pump-thaw cycles. The sample temperature was held constant at 50°C while water vapor exposures up to 10^9 L were given. The pressure in the microchamber was monitored by a Baratron capacitance manometer and ranged from 1.3×10^{-3} to 1.3 mbar depending on the exposure. The base pressure in the microchamber was 1×10^{-7} mbar.

Oxide nanostructures formed during exposures were subsequently characterized by x-ray photoelectron spectroscopy employing non-monochromated Al Kα radiation ($h\nu$ = 1486.6 eV). XPS spectra were recorded at normal emission geometry using fixed analyzer transmission mode with 20.0 eV pass energy. The analyzed area was 600 µm in diameter, so all results present an average over a large number of individual grains.

Data analysis

The principles of XPS data analysis are illustrated in Figure 1 using the O 1*s* photoelectron signal as an example. Figure 1(a) shows the analysis by least-squares fitting of synthetic Gaussian-Lorentzian lineshapes to the photoelectron peak after subtracting a Shirley background. The binding energy scale was referenced to the Fe 2$p_{3/2}$ transition of metallic iron at 707.0 eV. Chemical states of each element are identified from the spectra by the corresponding binding energies, and their relative concentrations are estimated by the integrated areas of the synthetic components. The O 1*s* signal after exposures to pure oxygen consisted of lattice oxygen

(O^{2-}, 530.4 eV) and adsorbed atomic oxygen (O_{ads}, 532.1 eV). After exposures to water vapor, lattice hydroxyl (OH^-, 531.7 eV), adsorbed hydroxyl groups (OH_{ads}, 532.5 eV) and molecularly adsorbed water (H_2O_{ads}, 533.7 eV) were also present.

The measured intensity of a photoelectron peak depends strongly on the depth of origin of the photoelectrons, since electrons traveling through a solid experience energy loss due to inelastic scattering events. Thus, without prior knowledge of the depth distribution of emitting atoms, the analysis as shows in Figure 1(a) is only semiquantitative. Information on the depth distribution is essentially contained in the energy loss structure that accompanies the photoelectron peaks. Hence, surface morphology (i.e., the depth distribution of the cations, anions and atoms) was determined by inelastic electron background analysis as illustrated in Figure 1(b) for the O 1*s* region. This method of quantification is based on the formalism developed by Tougaard and co-workers[6] and relies on accurate description of inelastic electron scattering. In practice the analysis is carried out by measuring reference spectra from pure elements or compounds and using this data to calculate a model spectrum for a given depth distribution and concentration. These parameters are then varied until the best agreement with the experimental spectrum is found.

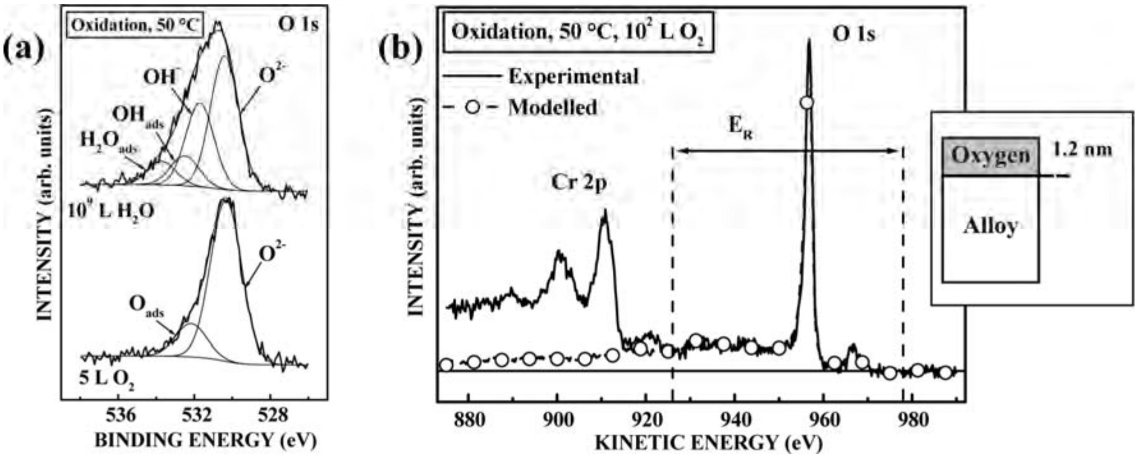

Figure 1. Analysis of the XPS data from the O 1*s* transition. (a) Analysis by least-squares fitting of synthetic lineshapes corresponding to the different chemical species found after 10^9 L H_2O and 5 L O_2 exposures at 50 °C. (b) Inelastic electron background analysis after 10^2 L O_2 exposure at 50 °C. E_R indicates the region used in the analysis of the oxygen signal. The baseline is a linear approximation of inelastic electron backgrounds originating from any peaks at higher kinetic energies. Model spectra for metallic Cr and Cr cations were used in the analysis of the Cr 2*p* signal but are excluded here for clarity.

Results and discussion

The chemical composition of the annealed Fe-17Cr surface was characterized by XPS prior to any exposure to oxygen or water vapor. Before each exposure, the surface consisted of 15–21 at.% Cr, 6 at.% C, and 6 at.% O (balance Fe) within the information depth of ~5 nm. Inelastic electron background analysis indicated that there was considerable chromium enrichment at the surface (37 at.% Cr in the topmost atomic layer) whereas the concentration decreased rapidly with increasing depth to 15 at.%. The lineshapes of the Cr $2p_{3/2}$ and Fe $2p_{3/2}$ photoelectron peaks indicated that no oxides were present at this stage.

Reaction with pure O_2

The growth of the oxide layer thickness upon exposure to pure O_2 at 50°C is shown in Figure 2. As seen from Figure 2(a), the annealed stainless steel surface is very reactive towards molecular O_2, and the initial oxidation is rapid until the oxide layer has reached approximately 0.7 nm thickness. At this stage, the initial oxide covers most of the surface, and further oxidation is hindered as it must proceed via transport of ions through the film. Upon increasing the exposure, the oxidation rate slows down further and a final thickness of 2.3 nm is reached as shown in Figure 2(b). Figure 2 also shows how the relative concentration of chromium cations within the oxide layer changes as the oxidation proceeds. Chromium is known to have higher chemical affinity to oxygen than iron does, and consequently the initial oxide structures (exposures up to 2 L) do not contain any iron cations.

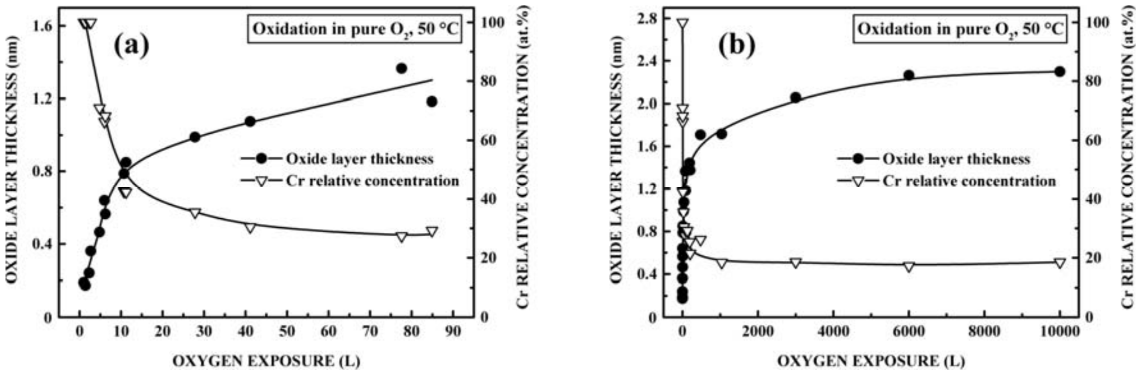

Figure 2. Oxide layer thickness and the relative concentration of Cr cations within the oxide film as obtained by inelastic electron background analysis after exposures to pure O_2 at 50 °C. Solid lines shown are only to guide the eye.

Nanoscale oxide structures formed on the annealed Fe-17Cr surface are shown schematically for selected exposures in Figure 3. The mobility of metal atoms is very low at 50 °C and thus the oxidation of Cr is kinetically constrained: the supply of metallic chromium at the surface is quickly consumed by oxide formation and a Cr-depleted region (~0.5 nm thick, 1–2 atomic layers) forms below the oxide (Figure 3(a)). As the O_2 exposure increases, the initially Cr-rich oxide becomes a mixture of Fe and Cr oxides, so that the final Fe/Cr ratio within the oxide corresponds closely to the bulk composition of the material (Figure 3(b)). Similar trends were observed in our previous studies of austenitic stainless steel surfaces.[7,8]

Reaction with water vapor

The surface was considerably less reactive towards water vapor than pure oxygen. All H_2O exposures from 10^5 to 10^9 L at 50°C produced a saturated chromium oxyhydroxide layer with ~0.6 nm thickness and containing no oxidized iron (Figure 3(c)). Adsorption of H_2O has been investigated previously on pure iron by Grosvenor and co-workers.[9] They concluded that the presence of hydrogen-containing species within the oxide hinders the transport of ions through the film, while their adsorption on the surface restricts the number of surface sites available for further adsorption. Similar mechanisms may be operative on the Fe-17Cr alloy surface as suggested by the chemical composition of the oxyhydroxide layer in Figure 1(a). Figure 3(d) shows the oxyhydroxide surface after further exposure to 10^2 L O_2 at 50°C, and comparison with Figure 3(a) indicates that the Cr-rich oxyhydroxide is indeed more resistant towards further oxidation than the oxide structures formed in pure O_2. Further experiments are needed in order to investigate the extent of this resistance and its dependence on temperature.

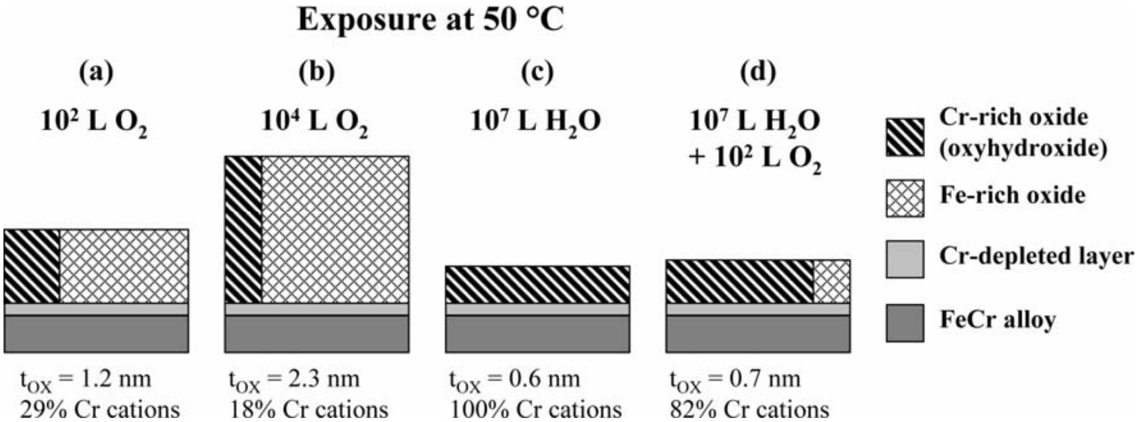

Figure 3. Surface morphology as determined by inelastic electron background analysis after various gas exposures at 50°C. t_{OX} is the thickness of the oxide layer. The thickness of the Cr-depleted layer is not shown to scale.

Controlling the ratio of H_2O and O_2 exposures could provide a means of controlling the chemical composition of the surface when investigating preparation of functional nanostructures. It should be noted that the reaction with O_2 dominates greatly over the reaction with H_2O, and thus H_2O would have little influence on the nanoscale oxidation of stainless steel upon co-adsorption of these gases.[10] Methods such as solution chemistry and plasma treatments can be used to increase the hydroxyl fraction on steel more effectively for, e.g., coating applications.[3]

Conclusions

XPS and inelastic electron background analysis have been employed to study the interaction of annealed Fe-17Cr surface with pure oxygen and water vapor. The nanostructures formed in pure O_2 at 50°C consisted of mixed iron-chromium oxides whereas those formed in water vapor consisted of chromium oxyhydroxide. The adsorption of water vapor hinders nanoscale oxidation, and doping the surface with hydroxyl groups could have significance for controlled adsorption of other molecules.

References

[1] K. Kolasinski: Surface science: Foundations of catalysis and nanoscience, John Wiley & Sons Ltd, UK 2002, pp. 31 – 68

[2] L. Pramatarova, E. Pecheva, and V. Krastev: "Ion implantation modified stainless steel as a substrate for hydroxyapatite deposition. Part II. Biomimetic layer growth and characterization", Journal of Materials Science: Materials in Medicine, 18, 2007, pp. 441 – 447

[3] J. Wielant, T. Hauffman, O. Blajiev, R. Hausbrand, and H. Terryn: "Influence of the iron oxide acid-base properties on the chemisorption of model epoxy compounds studied by XPS", Journal of Physical Chemistry C, 111, 2007, pp. 13177 – 13184

[4] I. Frateur, J. Lecoeur, S. Zanna, C.-O. Olsson, D. Landolt, and P. Marcus: "Adsorption of BSA on passivated chromium studied by a flow-cell EQCM and XPS", Electrochimica Acta, 52, 2007, pp. 7760 – 7769

[5] K. Lahtonen, M. Lampimäki, P. Jussila, M. Hirsimäki, and M. Valden: "Instrumentation and analytical methods of an x-ray photoelectron spectroscopy–scanning tunneling microscopy surface analysis system for studying nanostructured materials", Review of Scientific Instruments, 77, 2006, pp. 083901-1 – 083901-9

[6] S. Tougaard: "Accuracy of the non-destructive surface nanostructure quantification technique based on analysis of the XPS or AES peak shape", Surface and Interface Analysis, 26, 1998, pp. 249 – 269

[7] M. Lampimäki, K. Lahtonen, P. Jussila, M. Hirsimäki, and M. Valden: “Morphology and composition of nanoscale surface oxides on Fe-20Cr-18Ni{111} austenitic stainless steel”, Journal of Electron Spectroscopy and Related Phenomena, 154, 2007, pp. 69 – 78

[8] P. Jussila, K. Lahtonen, M. Lampimäki, M. Hirsimäki, and M. Valden: “Influence of minor alloying elements on the initial stages of oxidation of austenitic stainless steel materials”, submitted to Surface and Interface Analysis

[9] A. Grosvenor, B. Kobe, and N. McIntyre: “Studies of the oxidation of iron by water vapour using X-ray photoelectron spectroscopy and QUASES^{TM}”, Surface Science, 572, 2004, pp. 217 – 227

[10] C. Palacio, H. Mathieu, V. Stambouli, and D. Landolt: “XPS study of in-situ oxidation of an Fe-Cr alloy by low pressure oxygen in the presence of water vapor”, Surface Science, 295, 1993, pp. 251 – 262.

A CASE STUDY ON CORROSION OF STAINLESS STEEL IN FIREWATER MAINS

L. Carpén[1], T. Ohligschläger[2]

[1]VTT Technical Research Centre of Finland, Finland, [2]Outokumpu Stainless Oy, Finland

Abstract

Traditionally, many firewater mains were made of carbon steel or cast iron. At present, more and more stainless steel is used as material for firewater pipes due to usually better corrosion resistance in natural waters than iron or carbon steel. In some few cases, however, unexpected corrosion failures in systems using austenitic stainless steels were observed only after a relatively short time of usage ranging from a few weeks to a few years. Most of these corrosion damages were found on the weld nuggets or in the heat-affected zones of on-site girth welds. One of the most important factors affecting the corrosion resistance of stainless steel at welds and in heat-affected zones are the surface oxide films originating from the welding heat in the presence of oxygen (heat tints). Therefore, proper root shielding is important especially when welding pipes for fire protection systems where the water is taken from natural sources (e.g. from rivers, lakes or tap water), as microbially induced corrosion (MIC) can increase the risk for corrosion damages significantly. Two failure cases in fire protection systems, one in a stainless steel factory and one in a power plant have been studied and are described in this paper. A proposal for the mechanism is suggested and general recommendations how to avoid or diminish the risk for unexpected localised corrosion failures are given.

Introduction

Carbon steel or cast iron are traditional materials for firewater mains. Clogged tubes due to corrosion of these materials have caused problems over the years and alternative materials have been considered. Stainless steel has nowadays started to be used in firewater piping. Stainless steel has usually an excellent corrosion resistance in cold, flowing, low-chloride containing water. In stagnant water, like it is usually found in firewater systems, the corrosion resistance evidently diminishes. This is the case also when the temperature or the chloride content increases. Thiosulphate is known to have a detrimental effect on the pitting corrosion resistance of stainless steel if it exists in a proper ratio to chloride and/or sulphate [1,2].

Corrosion of stainless steels in natural waters and in systems using such water is typically localised corrosion. In welded structures, corrosion is often concentrated in the weld nugget itself or in the heat-affected zone. The openings of the corrosion pits are typically very small but large subsurface cavities are often formed. Especially on-site welds, like welded butt joints of pipes, are vulnerable to such pitting failures. On-site welds are usually welded from the outside of the pipe using shielding gas inside. Normally it is difficult or even impossible to clean the root of the weld after welding properly. If the shielding gas contains already a relatively small amount of oxygen, heat tint layers (coloured oxides) will be formed close to the weld. The pit initiation potential in these areas as well as on the weld itself is usually lower than on the base metal.

These heat tint layers promote the initiation and growth of corrosion pits even in seemingly harmless environments [3,4].

Natural waters contain always a diversity of microbes and thus these seemingly harmless environments might turn out to be aggressive. Microbes can change the environment's corrosiveness either chemically or physically. This phenomenon is called microbially induced corrosion (MIC). It is generally accepted that the ennoblement (increase of the open circuit potential) of stainless steel surfaces detected all over the world in ocean waters, brackish waters, rivers and even tap water is caused by microbial colonisation. This ennoblement can exceed the pit initiation potential. However, the mechanism of ennoblement is not clear and many different hypotheses and theories have been suggested during the years. One of these is the role of manganese oxidising bacteria, which can oxidise Mn^{2+} to the strong oxidant Mn^{4+} causing the potential of the metal to rise. Sulphate reducing bacteria (SRB) have often been detected together with iron and manganese oxidising bacteria on failure areas of stainless steels. SRBs can lower the redox potential within the deposits on the surface by producing sulphides (S^{2-}). Another way for SRBs to enhance the corrosion of stainless steel is to form thiosulphate ($S_2O_3^{2-}$). SRBs consume sulphate (SO_4^{2-}) by reducing it to sulphide, which can be oxidised to thiosulphate in the presence of air. In simulated paper machine water, it has been demonstrated that thiosulphate produced by the metabolic activity of SRBs caused severe pitting corrosion to stainless steel [2].

In this paper, failure analyses of two case histories of fire protection systems suspected to be caused by MIC are presented.

Case Histories

Case 1: Fire Protection System in a Stainless Steel Plant

The fire extinguishing system in a stainless steel plant had been earlier made of carbon steel and is gradually being changed to stainless steel type EN 1.4301. The removed carbon steel pipes were heavily corroded and had huge amounts of reddish brown deposit and tubercles inside the pipes after 20 years of usage. The examined stainless steel parts have been installed in the cold rolling plant in 2002 and some failures occurred after less than three years of usage. The raw water comes from a river nearby, is not specially treated and stays stagnant most of the time. The temperature varies from about 5-10ºC in some staircases during winter times to up to 50ºC over furnaces of the annealing lines. Stainless steel is also partly used in the hot rolling plant's fire protection system (FPS). The water comes from the same source but the water in the system is used for washing about once a week instead of the stagnant situation at the cold roll mill. No failures have been detected in these stainless steel pipings after over 15 years of usage. The chloride content of the river is usually very low (~1 mg/l). Only very seldom higher chloride values have been measured, when brackish water (~1000 mg/l of Cl^-) from the sea nearby is mixed with river water during times of strong southern wind. The sulphate content in the river water is also low (~3 mg/l); its alkalinity is low (~0.35 mmol/l) as well as its hardness (~0.17 mmol/l); pH is neutral (~7.0); the amount of manganese is low (~0.006 mg/l) and that of iron is rather high (~0.5 mg/l). The pressure in the system is 13 bar due to the height of some buildings.

Case 2: Fire Protection System in a Power Plant

In Case 2, the pipes of the system were also originally constructed from carbon steel and had been gradually replaced by austenitic stainless steel pipes (both EN 1.4301 and EN 1.4401). There were still some parts made of carbon steel or cast iron in the system and the water contained high amounts of precipitated iron. The water used in this fire extinguishing system was tap water with a low chloride concentration. The water was treated with chloramine when the system was filled with water. The water stayed stagnant most of the time and was changed only once a year. Unexpected pitting corrosion in stainless steel pipes of this FPS was observed after just a few years of service. The pits detected were situated in the welds or in the heat-affected zones. The first perforations were detected in EN 1.4401 stainless steel pipes after two years of operation. Later on, several pits causing leaks were also detected in the EN 1.4301 material. The pressure in the piping system was 10 bar and the temperature was ambient (20...25°C).

Experimental Procedures

Metal samples were removed from the systems and were examined visually and under a stereo-microscope. The chemical compositions of the pipe material and the weld metal were analysed with an optical emission spectrometer (OES). Metallurgical examinations consisted of optical light microscopy of cross sections prepared from the samples, scanning electron microscopy (SEM) studies from failure areas and energy dispersive spectroscopy (EDS) of corrosion products or of the deposits on the inner surfaces of the pipes. In Case 1, the metal samples were completely dry when arriving at the laboratory. Therefore, traditional methods like cultivation could not be applied to detect possible bacteria. However, preliminary trials with a new PCR-method were performed with one sample showing corrosion failure. In Case 2, microbiological assays were also performed. The total counts of aerobic and anaerobic bacteria and the amount of sulphate reducing bacteria were analysed by cultivation from the samples taken at site, from the water inside the pipes as well as from the deposits on the surfaces of the pipes. Samples were scraped from several places on the surface of the opened pipe. The system had been opened half an hour before the sampling.

Results

Case 1

The failures of the removed metal pipes (EN 1.4301) occurred in less than three years of usage. Some pits already perforated the pipe wall. Most of the corrosion attacks detected were either in the fusion line or in the heat affected zone, Figure1. Although the weld itself was uneven and partly incomplete in some cases, the corrosion did not occur especially in those areas. Instead, colourful heat tint areas could be seen on the failed pipes. The heat tint colours ranged from very dark blue to dark brown.

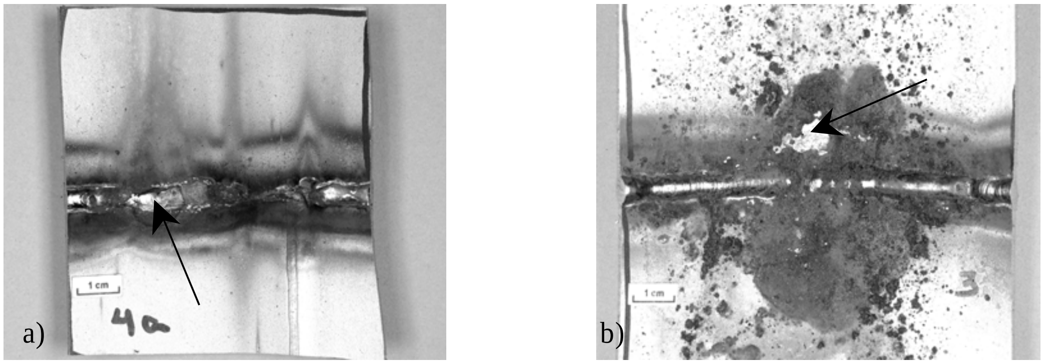

Figure 1. Pits (black arrows) a) in the fusion line and b) in the heat-affected zone of the weld.

For the common stainless steels types EN 1.4301 and 1.4401, it is usually considered that a slightly straw-yellow heat tint and otherwise clean weld indicate that the shielding gas protection has been satisfactory. All other colours indicate significant decrease in corrosion resistance [5]. In Figure 1a, also multicoloured areas linked to corrosion besides the heat tint areas can be seen. Iron, oxygen and carbon were the main elements of the EDS-analyses of the deposits on the inner surfaces. Moreover, chromium and nickel as components of stainless steel as well as manganese, sulphur and occasionally also phosphorus and chlorine originating from the environment were detected. High amounts of iron, manganese and chlorine had been detected earlier in deposits of MIC failure cases of stainless steels. Also the presence of sulphur and phosphorus can be regarded as an indication of bacterial involvement. Microbiological results taken from the failure area of one of the samples showed signs of bacteria. From this sample, bacterial DNA was isolated and multiplied with PCR using eu-bacteria primers. However, it was not possible to identify the different species without sequencing. The metallographic examination did not reveal any abnormalities in the normal austenitic microstructures of the studied samples.

Case 2

The first perforating pits in this fire extinguishing system were observed in a type EN 1.4401 stainless steel pipe with a diameter of 140 mm and a wall thickness of 3 mm. The leaks were situated near a girth weld. Visual inspection of the pipe sample revealed two perforations that were located in the heat-affected zone close to the fusion line of the on-site weld. Plenty of reddish brown deposit was found on the opposite inner side (Figure 2a). Similar reddish brown deposits and deposit rings were observed on the inner surfaces of type EN 1.4301 stainless steel pipes removed from the fire extinguishing system later. Typically, the openings of the pits were very small having large subsurface cavities (Figure 2b). The chemical compositions of the type EN 1.4301 stainless steel samples were according to the specifications within the ASTM standard boundaries except for some of the samples, which contained less than 18 % Cr (17 and 17.7 %). The microstructure of both materials was normal austenitic. The pits were typically situated close to or in the transversal on-site welds. There were clear signs of oxidation of heat-affected zones (heat tints) but no other signs for welding defects were found in the failure areas.

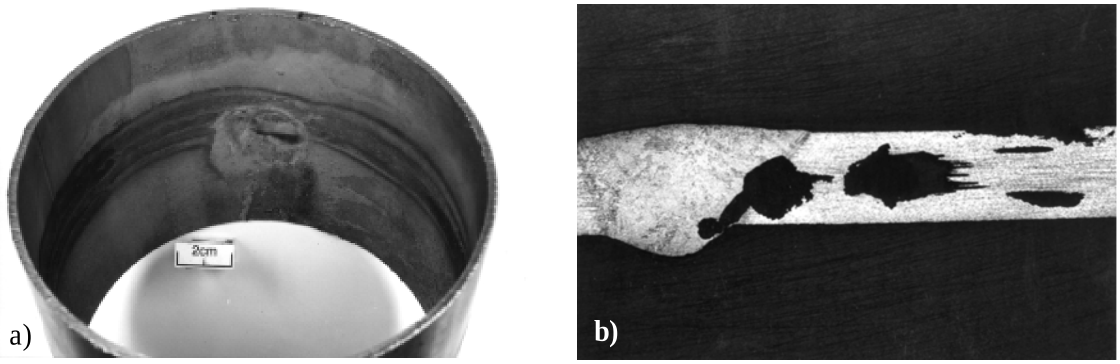

Figure 2. a) Reddish brown deposit on the inner surface of a stainless steel type EN 1.4401 pipe section removed from the fire extinguishing system. b) Optical micrograph of a trough-wall, mainly subsurface corrosion pit in an EN 1.4401 type of stainless steel pipe after two years of service in fire extinguishing water.

The pits were typically surrounded by dark brown circular deposit rings and the inner surfaces of the pipes were mostly covered with a thin and rather smooth layer of yellowish brown deposit. Sulphur and occasionally also high amounts of manganese as well as small amounts of phosphate were detected in the deposits in or surrounding the pits.

The results of the water analysis from a water sample taken a few months after the first leaks occurred (water A) is given in Table 1. In the same table, also the analysis of a water sample taken from the same fire extinguishing system two years later in relation to the leakage of the type 1.4301 pipes (water B) is listed. Waster C is used as feeding water for the fire extinguishing system and can be regarded as typical drinking water.

Table 1. Chemical analysis of the water samples taken from the fire extinguishing system of the power plant.

Water	pH	Fe mg/l	Mn mg/l	Ca mg/l	Mg mg/l	Cl^- mg/l	SO_4^{2-} mg/l	HCO_3^- mg/l	NO_2^- mg/l	NO_3^- mg/l
A	6.0	0.01	0.40	8.8	4.0	28	n.a.*	n.a.*	n.a.*	n.a.*
B	7.2	0.44	0.53	12.0	4.4	21	34	20	<0.01	1
C	7.8	0.05	0.02	12.0	4.7	24	27	26	<0.01	<1

* not analyzed

The total count of aerobic bacteria in samples taken directly from the surfaces of the opened system was clearly higher (from 1.1 x 10^3 to 7.3 x 10^3 cfu/ml) than in the water sample (32...50 cfu/ml). SBRs could be detected from the pipe sample, which had been delivered to the laboratory with a moist deposit still on its surface. Also the amount of aerobic bacteria in this sample was rather high, namely 4.3 x 10^6 cfu/cm^2, which was clearly higher than that in the pipe sample with dried deposit (20 cfu/cm^2). Both samples contained through-wall pits. The presence of iron bacteria was verified from the sample delivered to the laboratory and the water taken simultaneously from the fire extinguishing system under consideration. The amount of heterotrophic aerobic bacteria was quite high (4.3 x 10^5 and 2.4 x 10^5 cfu/ml respectively). Plenty of individual rod-shaped bacteria as well as cell aggregates and starting biofilm formation on the stainless steel coupons incubated six days in an iron bacteria culture medium could be seen under the epifluorescence microscope. The presence of manganese oxidising bacteria was not checked.

Discussion

Both failure cases occurred after a short time of usage in water with low chloride content. Under normal conditions, these types of water are not regarded as corrosive to the stainless steel types EN 1.4301 or EN 1.4401. However in these cases, the water was stagnant most of the time and only occasionally used. In stagnant waters with the possibility for deposit formation, the corrosion resistance of stainless steels is clearly diminished. During long stagnant periods, the stainless steel surface is not cleaned and bacterial activity may increase. The presence of bacteria was verified for Case 2 and indications of bacteria growth were found also in Case 1. It is generally accepted that the noble shift of the open circuit potential of stainless steels detected all over the world in natural waters is caused by microbial colonisation. This ennoblement can exceed the pit initiation potential even in low chloride waters. Usually the pit initiation potential on the weld and on the heat-affected zone is lower than on the base metal. Therefore, pitting corrosion starts often in these areas. Heat tint layers are also rich in iron and manganese oxides, which might explain why harmful bacteria tend to attach to these areas as well. Ennoblement alone cannot cause pitting corrosion. There has to be also some anions able to produce strong acid solutions inside the pit. Chlorides are the most common anions causing pitting corrosion of stainless steels by forming concentrated metal chloride solutions inside the pits. In typical pure drinking waters having low chloride concentrations (6...30 mg/l) the pitting potential for stainless steels at room temperature is very high (>1000 mV_{SCE}). In our earlier study [3], the effects of heat tints on pitting corrosion were examined in chloride solutions at room temperature. It was shown that pits could initiate at substantially lower potentials in heat tint areas than in areas without heat tints. However, the potentials required for continued growth of open pits in a dilute (106 mg/l Cl) plain chloride environment were considered still quite high for serious pitting in seemingly harmless environments to be explained by the presence of heat tints alone. In the presence of sulphates, the needed amount of chlorides to initiate corrosion is even higher and is depending on the molar ratio of chlorides and sulphates.

In many cases where pitting corrosion of stainless steels in fresh waters occurred, manganese and/or iron oxidising bacteria (like *Leptothrix*, *Siderocapsa*, *Gallionella*) had been detected. Iron oxidising bacteria can oxidize ferrous iron to ferric iron, which then reacts with the chloride ions producing ferric chloride [6]. Ferric chloride is extremely aggressive causing pitting corrosion on stainless steel. The deposits from the bacteria are rich in ferric chloride and attack aggressively austenitic stainless steels. Manganese oxidising bacteria oxidise Mn^{2+} to Mn^{4+}, which is a strong oxidiser as well. In the studied cases, indications of iron oxidising bacteria were detected from the deposits. The presence of manganese oxidising bacteria was not tested. Anaerobic SRBs were also found in failure areas often together with manganese- and iron-oxidising bacteria, as was shown also in our Case 2.

Another mechanism of how microbes can affect the initiation of pitting corrosion of stainless steels is the formation of thiosulphate. This type of pitting does not need the ennoblement of the steel but can occur at lower potentials than in pure chloride environments. SRBs consume sulphate by reducing it to sulphide and which in the presence of air can be oxidized to thiosulphate. During the stagnant periods in the system, anaerobic bacteria like SRBs produce sulphide. During occasional usage of the fire extinguishing system when oxygen or oxygen containing new water can enter the system, thiosulphate is formed. In simulated paper machine water, it has been demonstrated that thiosulphate produced by the metabolic activity of SRBs caused severe pitting corrosion of stainless steel type EN 1.4301 [2].

The waters in both cases contained also a high amount of precipitated iron. The high concentration of iron in the water can offer suitable conditions for iron oxidising bacteria. Besides iron hydroxides can behave as anion selective membrane at neutral pH and had been shown [7] playing a certain role for the occurrence of localised attack of stainless steel.

Conclusions and Recommedations

The influence of microbial activity played a decisive role in these pitting corrosion cases of stainless steel piping in firewater mains. The presence of precipitated iron and heat tint areas of welded structures increased the danger for corrosion failure.

The best way to prevent the formation of deleterious oxide layers is to remove oxygen from the piping by shielding gas flushing before welding and using backing gas during the whole welding process and some time afterwards. The oxidisation of the weld root can be reduced also by using root paste. This paste reacts with the welding heat and forms a slag layer on the root side of the weld. However, the results achieved with root paste are not anywhere near the results achieved by using backing gas. Alternatively, heat tints can be removed by pickling after welding. However, this is not always possible when considering the welding of piping containing natural waters. To avoid this kind of failures one should use water as clean as possible with low amounts of solids, chlorides, manganese and iron as well as a low amount of organic substances. Additionally, stagnant conditions or very low flow rates should be avoided as well. If continuous flow is not possible, the water should be changed frequently enough and the amounts of bacteria should be checked regularly. When necessary, the water should be treated to minimise bacterial activity. In Case 1, no failures had been detected in the system using the same water with regular use (once a week). In Case 2, the problems had been solved by using very clean demineralised water and circulation.

References

[1] A. Garner. “Thiosulphate Pitting of Austenitic Stainless Steels”, Corrosion Australasia, Feb. 1988, pp. 16-18.

[2] L. Carpén, L. Raaska, K. Kujanpää, K. Mattila, P. Uutela, M. Salkinoja-Salonen & T. Hakkarainen. “Simulation of MIC at splash zone areas of the paper industry.” CORROSION 2001, paper no. 245. Houston, Texas: NACE International; 2001.

[3] T. Hakkarainen and L. Carpén. “Effects of Heat Tints on Pitting Susceptibility of Stainless Steel.” Paper No. 061. 7th International Symposium on Electrochemical Methods in Corrosion Research, EMCR2000. Budapest, Hungary-May 28-1 June 2000; 2000.

[4] L.Carpén, L.Raaska, K.Kujanpää and T.Hakkarainen. “Effects of *Leptothrix discophora* on the potential behavior of stainless steel”. Materials and Corrosion 54, 515-519; 2003.

[5] Outokumpu Stainless Corrosion Handbook; 2004

[6] S.W.Borenstein. “Microbiologically influenced corrosion handbook.” Woodhead Publishing Ltd.; 1994.

[7] M.H.W.Renner. “Corrosion Engineering aspects regarding MIC related failures of stainless steels.” CORROSION 98, paper no. 285. Houston, Texas: NACE International; 1998.

HIGH TEMPERATURE BEHAVIOUR OF 22Cr-5Al STAINLESS STEEL IN WET AIR AND CO_2 ATMOSPHERES

A. Paúl[1,2], O.M. Montes[2], J.A. Odriozola[2]

[1]Universidad de Sevilla, Spain, [2]Universidad de Sevilla-CSIC, Spain

Abstract

In this work we study the effect of atmosphere composition on high temperature oxidation resistance of 22Cr-5Al stainless steels. Specimens were isothermally oxidised at 900ºC in CO_2, synthetic air and synthetic air containing H_2O during 22,7 hours in a thermobalance. The oxide layer formed over these samples after the oxidation was characterized with X-ray diffraction, scanning electron microscope, and glow discharge spectroscopy. Experimental results showed that the weight gains for samples oxidised in air and wet air are similar. The same sample oxidised in CO_2 showed a weight gain much lower although it suffered some scale spallation. Compositional and structural analyses showed that the oxides formed on stainless steel surface after oxidation were composed of very thin Al-rich oxides (Al_2O_3) of acicular form.

Introduction

22Cr-5Al ferritic stainless steels are also known as Fecralloy (Fecralloy is the registered trademark of the UK Atomic Energy Authority, Now AEA Technology, Harwell). Is used in high temperature applications in several environments in domestic and industrial applications. The presence of Al (5%) and Y (0.1%) in the chemical composition is the key to its excellent resistance to high temperature oxidation to temperatures as high as 1200ºC. That resistance is due to the formation of a Al_2O_3 scale and the beneficial effect of the formation of Y_2O_3 that changes the diffusion mechanism and increases the scale adherence in what is known as the *reactive element effect* [1-3].

Traditionally Al bearing ferritics were used in furnace components, automobile exhaust and other high temperature applications in several aggressive environments. Recently the use of these alloys is being extended to other applications in which the metallic alloy acts as a support for ceramic functional materials: support for the deposition of hydroxyapatite in biomaterials; metallic monolithic catalyst support and other catalytic applications [4, 5].

Many of these new uses depend on the surface properties of the alloy: scale composition, morphology and adherence, which are a function of the heat treatment, temperature, time and atmosphere composition.

In this work we study the effect of atmosphere composition in the high temperature oxidation of 22Cr-5Al dedicating special attention to the structure composition and morphology of the scale formed. Pure CO_2, air, and wet air are used to oxide 22Cr-5Al ferritic stainless steel samples at 900ºC during 22.7 hours.

Experimental

Specimens of commercial grade 22Cr-5Al stainless steel (Goodfellow) were used in this work. Samples were extracted from 1 mm thickness sheets by shearing 15×15 mm samples. Edges were mechanised to the final dimensions, 13×13×1 mm and the all the surfaces of the specimen were grinded up to #600 grit SiC paper. Chemical composition as given by the manufacturer is indicated in table 1.

Table 1. Chemical composition (wt. %) of the 22Cr-5Al ferritic alloy used in this work.

Fe	Cr	Al	Y	Zr
72.8	22	5	0.1	0.1

The isothermal oxidation of each sample was carried out at 900ºC in a thermobalance (SETARAM TGDTA-92) during 22.7 hours under CO_2, synthetic air or synthetic air containing H_2O. In the latter, synthetic air flowed through a saturator immersed in a mixture of ice and water inside a Dewar recipient. At this temperature water vapour pressure is 6×10^{-3} bar. Thermogravimetric measurements were performed with a sensitivity of 0.01 mg and temperature control of ±0.01°C. The temperature rate between room temperature and 900ºC was 100°C min^{-1}. After placing the specimen in the thermobalance the device was flushed with the gas to be used in the experiments for 10 min at room temperature to purge residual air in the furnace chamber.

The samples were characterized after high temperature oxidation by several surface techniques: scanning electron microscope and energy dispersive X-ray spectroscopy (SEM/EDS) and glow discharge optical emission spectroscopy (GD-OES). A JEOL 5400 instrument was employed for Scanning Electron Microscopy experiments. It is equipped with an Energy Dispersive X-ray Spectrometer (OXFORD LINK *TETRA 1128-231*) operated at 20 kV. For transversal section studies with SEM the scale must be protected to avoid descaling during grinding and polishing. To do this the sample is electrolitically coated with Ni. GD-OES depth profiling was used to provide quantitative information of the in-depth scale composition. The GDOES analyses were performed using a current of 20 mA and a voltage of 700 V. The pressure was 10 torr. The area analysed by GDS is a 4mm diameter circle so it gives average macroscopic information of the scale.

Results and discussion

Figure 1 shows mass gain as a function of time for the samples oxidised in air, humid air and CO_2 at 900ºC. It can be observed that the weight gain of the samples oxidised in air and air containing H_2O are very similar. On the contrary the sample oxidised in CO_2 shows a different behaviour, rapidly increasing the mass gain initially an then changing to a asymptotic kinetic. This sample suffered some scale spallation during cooling. Total mass gain after 22.7 hours oxidation at 900ºC are shown in table 2. Thickness data are obtained supposing that the scale is formed only by Fe_2O_3 or Cr_2O_3.

Table 2. Mass gain and equivalent thickness of the specimens studied in this work.

Atmosphere	ΔW (mg cm^{-2})	x (μm)
Air	0,242	1.307
Air+ H_2O	0,233	1.258
CO_2	0,127	0.686

For the specimens oxidised in synthetic air and synthetic air containing H_2O oxidation kinetics indicates protective rate behaviour according to Wagner's parabolic law [18]. Both samples have similar behaviour and total mass gain values are comparable. The alloy oxidised in humid air seems to have a higher rate initial oxidation that will slow down later as compared to the sample exposed to pure synthetic air. This indicates the rapid formation of a protective layer. The sample exposed to CO_2 has less mass gain and a behaviour that is not strictly parabolic, the kinetic curve follow an asymptotic trend. Initially, the mass gain is very quick and after a few hours the oxidation rate is very low as total mass gain value indicates.

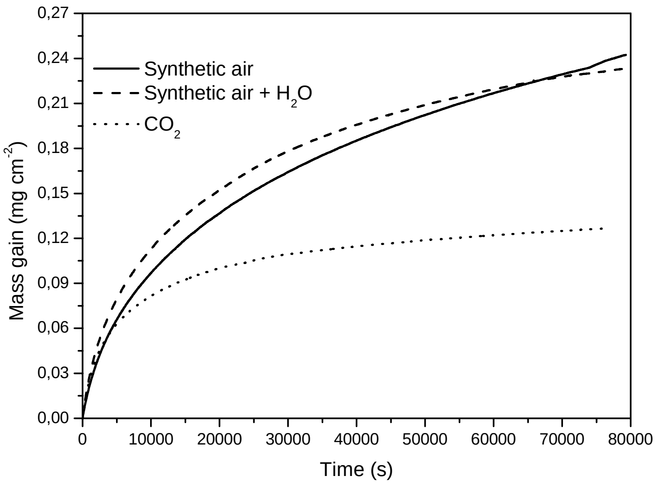

Figure 1. Thermogravimetric curves of 25Cr-5Al ferritic stainless steel specimens oxidised during 22.7 hours in different atmospheres.

SEM-EDX examination of the oxidised specimens is presented in figures 2-4. Scale morphology for all the samples is very similar. The oxide layer is formed by very small thin and flat Al_2O_3 oxides. The oxide grows towards the outside in normal direction so that only their thinnest face is seen giving the image of needle-like oxides. In the base of these oxides, below the needles, a layer of small oxide grains can be seen. In the sample exposed to humid synthetic air, figure 3, the flat crystals are less defined and the outer scale is more dense than in the other specimens. The samples oxidised in the presence of air, both dry and humid, also present some oxide nodules which, as analysed by EDX, revealed to be Fe-rich. These structures appear isolated in the surface and were not seen in the specimen exposed to CO_2 atmosphere. In that sample, figure 4, larger areas of flat oxide formation appear aligned with the surface scratches formed by the grinding process. EDX microanalysis of these formations indicates that they are formed by aluminium oxide Al_2O_3.

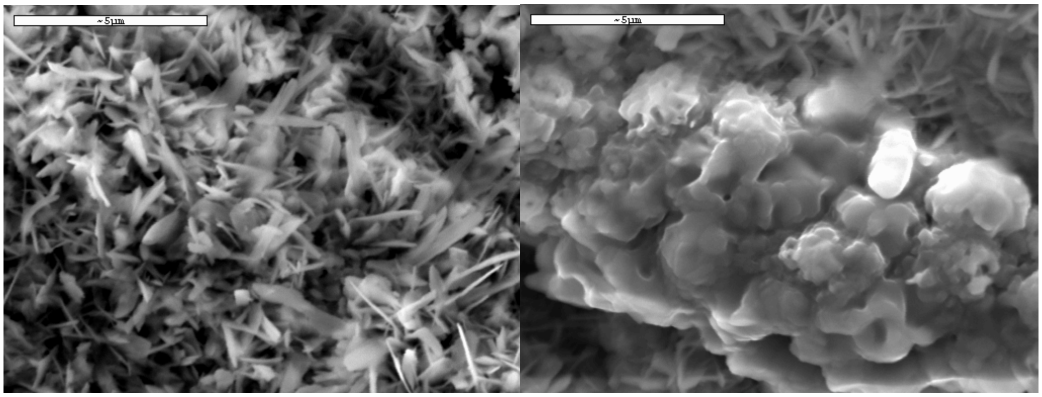

Figure 2. SEM images of the scale formed on the sample oxidised in dry synthetic air during 22.7 hours at 900ºC. Left general scale morphology, right detail of a Fe-rich blister.

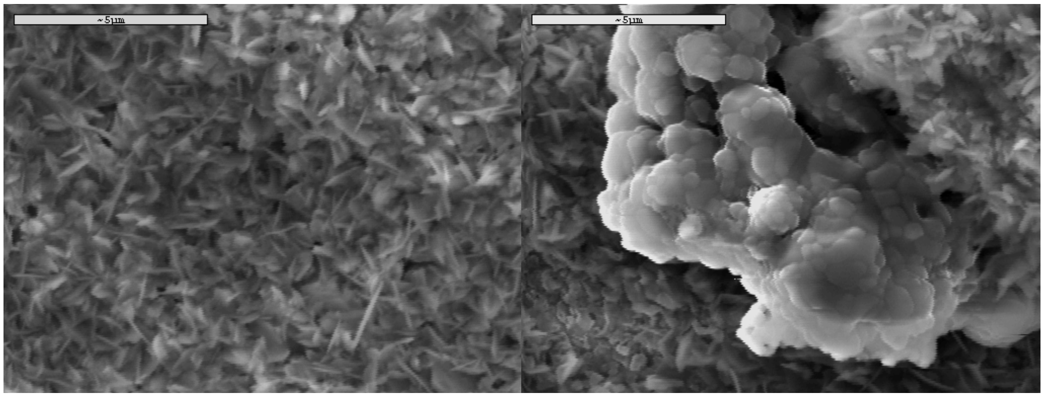

Figure 3. SEM images of the scale formed on the sample oxidised in humid synthetic air during 22.7 hours at 900ºC. Left general scale morphology, right detail of a Fe-rich blister.

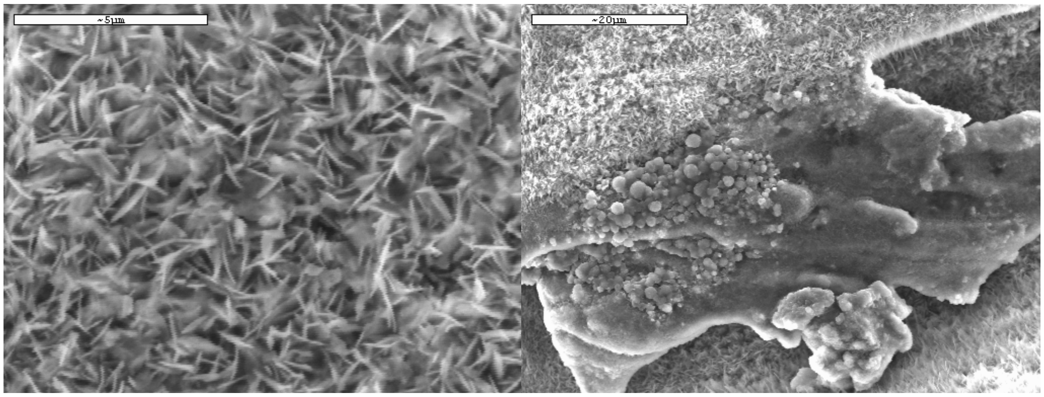

Figure 4. SEM images of the scale formed on the sample oxidised in CO_2 during 22.7 hours at 900ºC. Left general scale morphology, right detail of an Al-rich oxide formation.

GD-OES experiments were performed in order to obtain more information on the scale structure and chemical composition. Results are shown in figures 5-7. In all the samples is evident a large concentration of Fe and Cr in the outermost part of the scale. No oxygen is present in that zone. This is due to the effect of scale spallation. The plasma ignition process in the DGS lamp is produced in that areas so only metallic species are sputtered initially. Later, the plasma stabilization throughout the surface will produce the right depth profile, so that the specimen surface must be considered just below the Fe and Cr outer peak. Also the height of the Cr and Fe signal in that zone will be proportional to the extent of the surface spalled indicating that spallation is slightly stronger in the specimen oxidised in CO_2 than on the other amples. Also the spallation in humid air is larger than in the dry air specimen. Figure 5 presents the in-depth scale distribution of the atomic species in the specimen exposed to dry synthetic air. Results indicate that the scale is formed Al oxide, Al_2O_3. Total scale thickness is about 4.5 μm.

In figure 6 the results of GD-OES corresponding to the specimen exposed to humid air are presented. The scale structure is very similar to that of the previous samples confirming the results of SEM-EDS, the scale is formed by Al_2O_3. The thickness of the oxide layer is also very similar to the previous one.

The results for the alloy oxidised in CO_2 are presented in figure 7. They show that the scale in this sample does not differ much from the previous ones. Total thickness is similar, 4.5 μm. Also a higher Al content is detected on that sample.

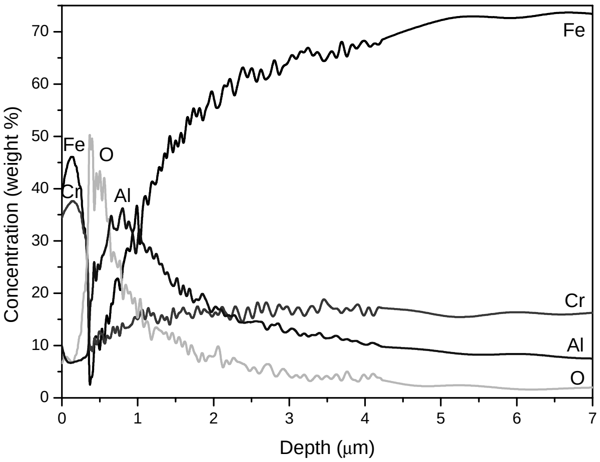

Figure 5. Depth profile composition in the scale formed on the specimen oxidised in dry synthetic air.

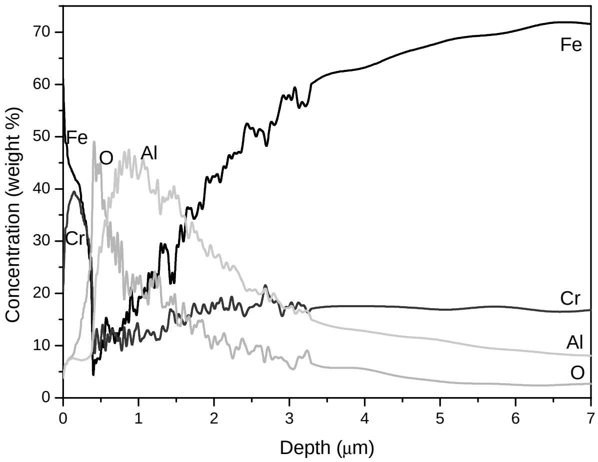

Figure 6. Depth profile composition in the scale formed on the specimen oxidised in humid synthetic air.

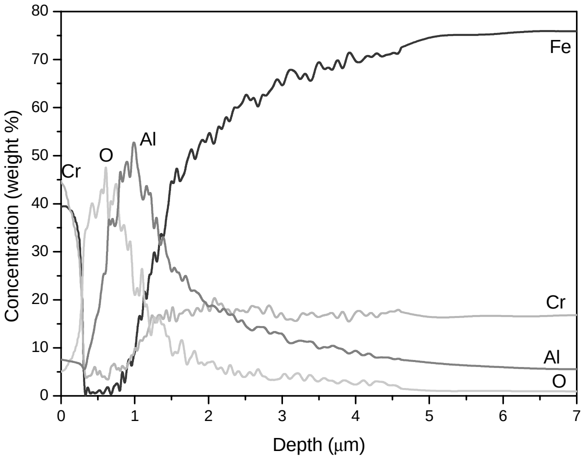

Figure 7. Depth profile composition in the scale formed on the specimen oxidised in CO_2.

Results of thermogravimetry experiments indicate a lower oxidation of the scale in the CO_2 oxidised specimen while SEM observation clearly shows some large oxide formations and GD-OES depth profiles shows a scale structure and composition very similar to that of the other samples. The reason of this seem to be the larger aluminium migration to the surface, the lighter weight of this element gave a thicker Al_2O_3 inner layer but less total mass gain. Also some reaction with the carbon present in the atmosphere and Cr (or Fe) present in the scale cannot be discarded.

Some differences are observed on the TG results of the samples oxidised in air that is not revealed by the SEM observation. The lower final weight gain and the change in oxidation kinetics observed for the sample oxidised in synthetic air with some water content can be related to the formation of volatile species such as $CrO_3(g)$, $CrO_2OH(g)$ or $CrO_2(OH)_2(g)$ that causes the evaporation of Cr_2O_3 scales at high temperature. That will give lower oxidation rates in the TG experiments as some mass loss is taken place by that processes.

The general morphology of the scales, composed of very thin oxide grains and porous structure, make these treatments useful for catalytic applications where a large area is required. For other applications where the morphology is less important and the scale adhesion is determinant, the treatments in CO_2 are not recommended.

Conclusions

The results of this study show the influence of atmosphere on oxidation of a 22Cr-5Al ferritic stainless steel. Specimens were oxidized at 900ºC for 22.7 hours in three different atmospheres: CO_2, synthetic air and synthetic air containing H_2O. Results of this work indicate that there are not many differences in the scales formed on 25Cr-5Al ferritic stainless steel after exposure to synthetic air, humid synthetic air and CO_2.

The weight gains obtained in air and air containing H_2O were higher than those in CO_2. Nevertheless the scale structure and morphology is independent from the oxidation atmosphere to which the samples where exposed.

These treatments are useful for applications where a large surface effective area is required while in other applications where scale adhesion is more important the preoxidation treatment studied in this work should be more controlled, specially the presence of C in the atmosphere.

REFERENCES

[1] P. Kofstad. High-temperature corrosion. Elsevier, London- New York (1988).
[2] D.R. Baer. Applications of surface science **7** (1981) 69.
[3] M. Thiele, H. Teichmann, W. Quadakkers. VGB Kraftwerkste **2** (1997) 77.
[4] X. Guo, J. Gough, P. Xiao. J. of Biom. Mater. Res. A **80** (2006) 24.
[5] D. Ugues, S. Specchia, G. Saracco Ind. Eng. Chem. Res. **43** (2004) 1990.

CORROSION RESISTANCE OF WELDED STAINLESS STEEL REINFORCEMENT IN CONCRETE

M.J. Correia[1], M.M. Salta[1], I.T.E. Fonseca[2]

[1]Laboratório Nacional de Engenharia Civil, Portugal, [2]Faculdade de Ciências da Universidade de Lisboa, Portugal

Abstract

The main goal of this paper is to assess the corrosion resistance in concrete of welded austenitic stainless steel alloys. The performance of alloys has been evaluated both in saturated calcium hydroxide solution and in concrete slabs periodically exposed to a 3% chloride (NaCl) solution. The potential monitoring and electrochemical periodic measurements in concrete showed that all welded stainless steel samples have a greater susceptibility to pitting corrosion comparatively with the respective unwelded samples. However, this difference is attenuated or even inexistent for welded polished samples, which are characterized by potentiodynamic polarization tests carried out in saturated $Ca(OH)_2$ solution with 10% chloride addition. This fact stands for the primary influence of the surface condition on the corrosion resistance of the stainless steel welded samples.

Introduction

Since reinforcement corrosion has become the most serious cause of premature deterioration of concrete structures, the corrosion prevention of reinforcements is crucial to preserve the durability of structures. Reported as a solution to achieve a maintenance-free long life construction, stainless steel reinforcement has been widespread in the last few years as an attractive technical approach to prevent corrosion.

The corrosion rate of stainless steel is significantly lower than that of carbon steel in aggressive environments and the threshold level of chloride content is several times higher than the amount necessary to initiate corrosion for the carbon steel rebar in concrete [1]. References are made to the experimental verifications that the critical chloride content for rebars embedded in chloride containing uncarbonated concrete may be as more than ten times higher for stainless steel as that for carbon steel [3-6]. Despite the high corrosion resistance shown by stainless steel it remains susceptible mainly to localized corrosion, pitting being one of the main forms of corrosion in an alkaline medium. Besides the environmental variables (temperature, pH, …), the material properties (composition, microstructure, surface condition, …) are critical conditioning factors of the stainless steel rebar pitting corrosion resistance behaviour. Then, the local microstructural and surface state modifications induced by welding can cause a variation in the corrosion behavior of any stainless steel alloy . The documented poorer performance of welded samples is generally attributed to the presence of mill scale and temper colours on stainless steel surface [1,6-9], their corrosion resistance being improved by pickling or blasting [1,7,8]. Regardless of the general agreement concerning the causes for the decrease in corrosion resistance of stainless steel welded samples, the research concerning this subject sustains an increasing knowledge, which is fundamental to implement specifications for the use of stainless steel in concrete.

In this study, the corrosion resistance in concrete of welded samples was assessed and compared with the behaviour of the respective unwelded austenitic stainless steel alloys: one conventional Fe-Cr-Ni base alloy (1.4301) and two lately developed Fe-Cr-Mn base alloys [10].

Experimental

Electrode materials

Three austenitic stainless steel alloys, one Fe-Cr-Ni alloy (1.4301 according to EN10088-1:2005; identified as SS0), and two newly developed high manganese alloys (SS1 and SS2), were tested. Table 1 indicates the chemical composition of the steel alloys studied.

Manual metal arc welding (316 electrode) was the procedure used to prepare the welded electrodes, which were afterwards cleaned with a brush.

Table 1. Chemical composition of steel alloys (weight %).

	C	**Mn**	**Si**	**P**	**S**	**Cr**	**Ni**	**Mo**	**N**	**Cu**
SS0	0.050	1.49	0.39	0.04	0.010	18.21	8.50	0.430	0.077	0.36
SS1	0.070	8.14	0.19	0.02	<0.001	16.52	0.22	<0.005	0.158	1.94
SS2	0.040	8.26	0.15	0.01	<0.001	16.50	1.23	1.930	0.290	2.06

Microstructural analysis

The microstructures of materials, before and after welding, were observed on an Olympus PMG3 metallographic microscope, after grinding, polishing with emery paper and diamond paste down to 1 μm, and appropriate etching. The stainless steel alloys were electrolyticly etched with a 10% oxalic acid solution. The grain size was characterized by comparison (ASTM E 112-96).

Electrochemical measurements

The electrochemical experiments were performed with a PCI4/300 Gamry electrochemical system.

Tests in concrete

For the tests in concrete, unwelded samples with 8 cm length were cutted from each stainless steel ribbed bars (ϕ 12 mm). Welded samples consist of two ribbed pieces of each alloy, with 4 cm length, but joint to each other. Welded and unwelded samples were assembled to a mould to achieve a 10 mm concrete cover in concrete slabs (30x30x10 cm). However, the welded area, due to its irregular shape, has, on some areas, a minimum 6 mm concrete cover.

The embedded steel samples have been exposed periodically to a 3% sodium chloride solution in alternated dry/immerson cycles, being monitored since the 41th day from the exposure beginning. These samples have also been submitted to periodic electrochemical tests, which started before exposure to NaCl solution. The half-cell potential of each sample was monitored, relatively to an embedded titanium electrode, with an Hp 34970A data acquisition switch unit. For these electrochemical tests, a stainless steel mesh and saturated calomel (SCE) were respectively used as counter and reference electrodes. The polarization resistance was done at 4.17×10^{-2} mV s^{-1} scan rate from -10 mV to + 10 mV relatively to the open circuit potential (OCP).

Potentiodynamic tests in $Ca(OH)_2$ saturated solution

The electrochemical experiments were conducted on a three electrode electrochemical cell in saturated $Ca(OH)_2$ solution (pH≈12.6) with 10% chloride, at room temperature. Disc shaped working electrodes (length = 2 mm; diameter = 10 mm) were prepared from ribbed bars from SS0 and SS1 stainless steel alloys. Welded disc shaped working electrodes were prepared, from the welded area of SS0 and SS1 welded samples, with lengths ranging from 2 to 5 mm. Prior to the experiments, each electrode was polished with emery paper down to 8.4 μm and with diamond paste down to 0.25 μm. Platinum and SCE were respectively used as counter and reference electrodes. The anodic polarization was done at 1 mV s^{-1} scan rate from -50 mV relatively to the open circuit potential (OCP) towards the transpassivation (Et) or pitting potentials (Ep). The scanning was reverted or stopped when reaching 20 μA cm^{-2} of current density, respectively when transpassivation or pitting potentials were attained.

Results

Microstructural analysis

Figure 1 shows the cross section microstructure of each studied alloy. All alloys show an austenitic matrix, and the high manganese alloys show also some local grain boundary carbide precipitates and ferrite. In particular, the SS2 alloy presents an uneven distribution of second phase particles, showing a clear reduction in their amount from the centre to the transversal section surface.

The welded area consists of three distinct zones: weld metal; heat affected zone; base metal. The microstructure of the weld metal solidifies as primary δ ferrite, which, upon cooling, becomes austenite and vermicular ferrite.

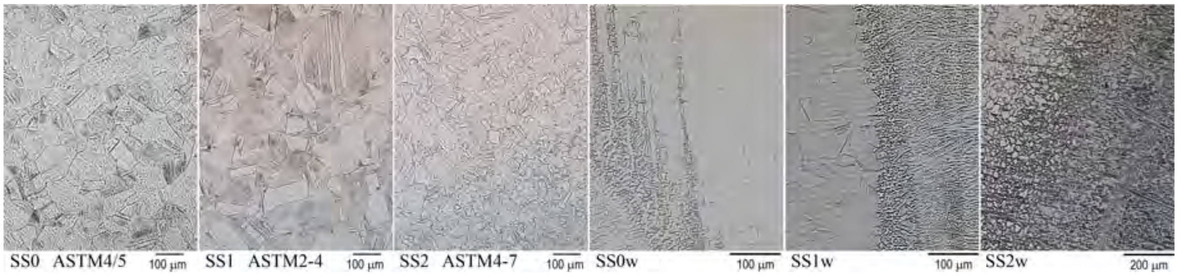

Figure 1. Microstructure of each alloy and of the welded area in each welded sample.

Potential monitoring and corrosion resistance in concrete

Figures 2 and 3 show the half-cell potential monitoring results of both stainless steel welded and unwelded samples, respectively.

Since the monitoring beginning, a reduction (in cathodic direction) in the half-cell potential of SS1 welded sample has been detected, to potentials more negative than -250 mV$_{TiA}$. The remaining welded samples (SS0 and SS2) show sharp cathodic potential decays each followed by a return to the original level as a result of repassivation. The welded SS2 high manganese sample exhibited, at 62nd and 340th days of exposure, long propagation periods of pitting corrosion. However, the stable pitting events have been followed by repassivation evidenced by the potential return to values higher than -100 mV$_{TiA}$.

During most of the exposure period, the unwelded stainless steel samples reveal a passive behavior, by showing half-cell potential values between 0 and -100 mV$_{TiA}$. However, it is also possible to notice a few transient decays in the half-cell potential of high manganese stainless steel samples. These features can be hypothetically considered to be due to nucleation of pits, and following repassivation.

The periodical electrochemical experiments give further support to the half-cell potential monitoring results. Polarization resistance results, indicated in Figure 4, evidence the active corrosion and the periodical activation of SS1 and SS2 welded samples, respectivelly. The half-cell potential and the polarization resistance values of SS1 welded sample have been less than -300 mV$_{SCE}$ and 10^5 Ω cm^2 respectively, except during the most recent days of exposure. The SS2 welded sample potential instability demonstrated the existance of transient events consisting of pitting corrosion initiation and following repassivation. Since this alternating active/passive behavior can only be detected by the periodical electrochemical tests for the longer transients, the hypothesis concerning the SS0 similar transition between pitting corrosion and repassivation was not confirmed. However, the equivalent features of the half-cell potential monitoring indicate a similar occurrence of metaestable pitting events.

Considering the cover thickness unevenness (6 to 10 mm), the chloride determination on the steel/concrete interface indicated a percentage by concrete mass between 0.3 and 0.5%, at the 50th day of exposure, and with an aproximatelly constant average value of 0.6% after 1 year.

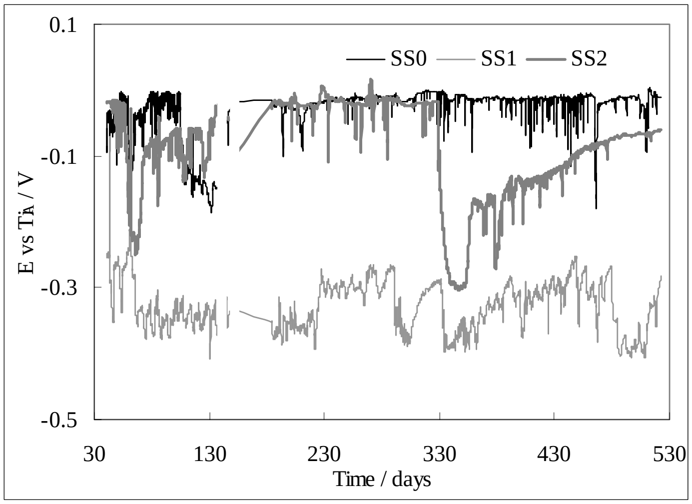

Figure 2. Half-cell potential of stainless steel welded samples in concrete submitted to cycles of exposure to a 3% sodium chloride solution.

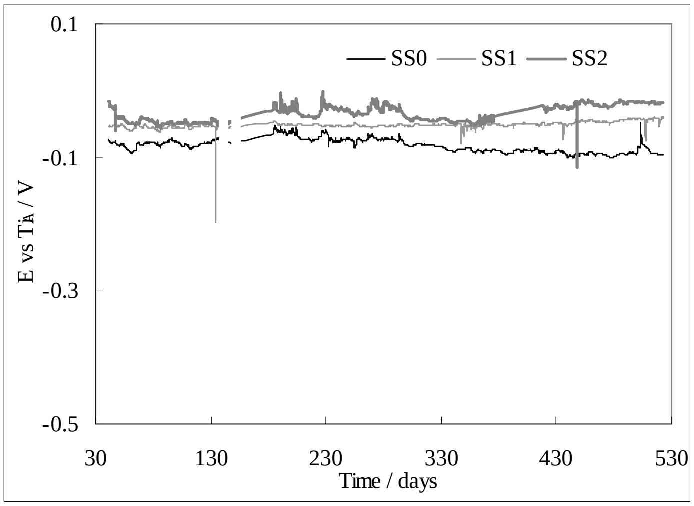

Figure 3. Half-cell potential of stainless steel samples in concrete submitted to cycles of exposure to a 3% sodium chloride solution.

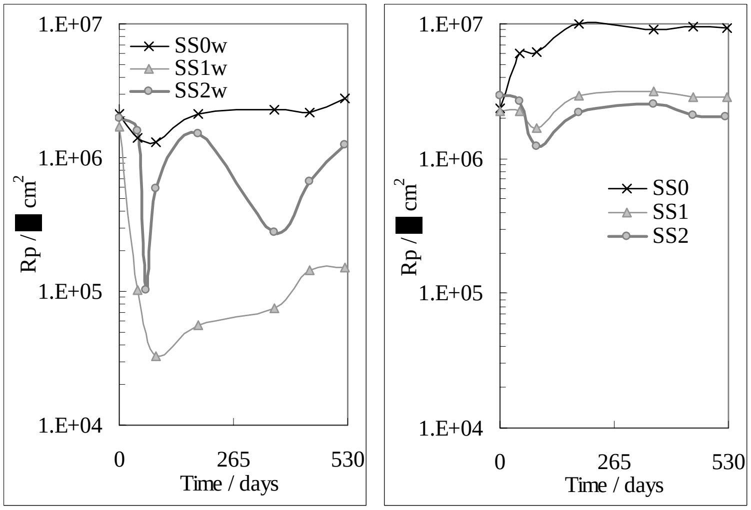

Figure 4. Periodical polarization resistance results for stainless steel welded (w) and unwelded samples in concrete.

Pitting corrosion resistance in $Ca(OH)_2$ saturated solution

Figure 5 illustrates the potentiodynamic curves (log I *vs* E plot) of welded and unwelded SS0 samples in $Ca(OH)_2$ saturated solution with 10% chloride addition (NaCl). According to the results illustrated in this figure, the unwelded SS0 stainless steel sample is resistant to localized corrosion under the studied conditions.

In saturated $Ca(OH)_2$ solution with 10% chloride addition, both welded austenitic alloys are susceptible to localized corrosion when the pitting potential is exceeded. This susceptibility was evaluated by the pitting potentials, indicated in Table 2. According to these results, the SS1 unwelded sample is also vulnerable to pitting corrosion, and shows similar pitting potential to the welded sample.

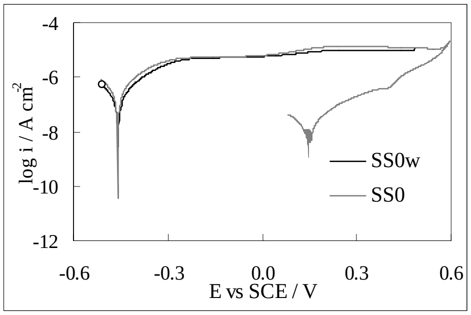

Figure 5. E *vs* log i plot of SS0 welded and unwelded samples in $Ca(OH)_2$ sat. solution with 10% Cl^-.

Table 2. Open circuit (Eoc), and pitting (Ep) or transpassivation (Et) potentials of stainless steel alloys in $Ca(OH)_2$ sat. solution with 10% Cl^-.

	Eoc mV *vs* SCE	Ep	Et
SS0	-452	-	593
SS0-w	-437	456	-
SS1	-406	472	-
SS1-w	-421	473	-

Discussion

Since the monitoring beginning, the welded samples have shown, in concrete, a susceptibility to pit and then a worse behaviour than the unwelded samples, which have maintained their passivity. Welded bars show a poorer performance than unwelded bars because the corrosion resistance of stainless steels is affected by the presence of mill scale and temper colours on their surface [1,6-9]. These are probably the main reasons for the differences found in this study between the behavior of welded and unwelded samples in concrete.

The distinct stainless steel samples show similar transient events, however, their propagation is favored on the high manganese alloys, especially on SS1. During melting, which fuses the base metal and filler metal, a zone is produced with a composition that is generally different from that of the base metal. This generates a galvanic couple, which can influence the corrosion process in the vicinity of the weld. This galvanic effect, which is more significant in the high manganese alloys, may justify the comparatively worse behavior of these alloys in concrete. After the pitting nucleation, the galvanic effect may stabilize the pit propagation, leading to long lasting stable pitting corrosion events in the high manganese alloys.

The corrosion resistance of welded bars is improved by pickling or blasting [1,7,8]. In this study, the surface was only brushed to remove some of the welding slag. Since the pitting corrosion resistance is highly influenced by the surface state, the surface irregularities, besides the mill scale and temper colours, are the reasons that explain the relatively better behaviour of welded samples found in solution. Nürnberger stated that under practical conditions of highly chloride contaminated uncarbonated concrete (up to 5% of chloride content) no risk of corrosion was exhibited by welded stainless steel type 1.4571 and type 1.4462 [2]. The results of this study obtained in solution also stand for the high corrosion resistance of welded samples.

Under the studied experimental conditions, the SS0 stainless steel alloy is the most resistant to pitting corrosion. This alloy, in alkaline solution with 10% chlorides, does not show susceptibility to pitting corrosion. The pitting potential of the welded samples is similar and comparable to the pitting potential of SS1 unwelded sample, which means that under similar conditions of induced polarization all these samples are equally susceptible to pitting corrosion. In $Ca(OH)_{2\ sat.}$ solution with 10% chlorides, both welded samples (SS0 and SS1) only pit for potentials exceeding 450 $mV_{SCE,}$ which are uncommon for the stainless steel alloys in concrete. The similar behavior found between the distinct welded samples and the unwelded SS1 sample, and the resistance to corrosion, unless when the high pitting corrosion potential is exceeded, determine the critical influence of the surface condition on the nucleation of the pitting corrosion process.

Conclusions

The results obtained in this study confirm the critical influence of the surface condition on the pitting corrosion initiation. A proper cleaning procedure after welding and the avoidance of surface irregularities, which can promote a localized concentration cell are extremelly important procedures to prevent the pit nucleation in the welded stainless steel samples. Another critical factor is the proper selection of the welding electrode, which can prevent one of the major sources of galvanic effects.

The welded and unwelded samples can have a similar corrosion resistance, as proven to be the case in alkaline solution, if proper care is taken with the above mentioned critical factors.

The high manganese stainless steel welded samples, and especially the SS1 welded sample, sustain stable propagation of pitting corrosion for longer periods, being for that considered as less resistant to corrosion than the SS0 welded sample.

Acknowledgements

Financial support to a PhD grant (SFRH/BD/19494/2004) from *Fundação para a Ciência e Tecnologia (FCT)* and *Laboratório Nacional de Engenharia Civil (LNEC)* are gratefully acknowledged.

References

[1] U. Nürnberger: "Stainless steel in concrete, EFC-18, The Institute of Materials, London, 1996.

[2] U. Nürnberger: “Supplementary corrosion protection of reinforcing steel”; Otto-Graf-Journal, 11, 2000, pp. 77.

[3] D. B. MacDonald, M. R. Sherman, D. W. Pfeifer and Y. P. Virmani: “Stainless Steel Reinforcing as Corrosion Protection”, Concrete International, May, 1995, pp. 65-70.

[4] M. C. García-Alonso, J. A. González, J. Miranda, M. L. Escudero, M. J. Correia, M. M. Salta and A. Bennani: “Corrosion behaviour of innovative stainless steels in mortar”, Cement and Concrete Research, 37, 2007, pp. 1562-1569.

[5] M. C. García-Alonso, M. L. Escudero, J. M. Miranda, M. I. Vega, F. Capilla, M. J. Correia, M. M. Salta, A. Bennani and J. A. González: “Corrosion behaviour of new stainless steels reinforcing bars embedded in concrete”, Cement and Concrete Research, 37, 2007, pp. 1463-1471.

[6] Report of a Concrete Society Steering Committee: “Guidance on the use of stainless steel reinforcement” - Concrete Society Technical Report 51, 1998.

[7] L. Bertolini, B. Elsener, P. Pedeferri and R. Polder: Corrosion of steel in concrete – Prevention, Diagnosis, Repair, WILEY-VCH, Weinheim, 2004.

[8] COST 521: “Corrosion of steel in reinforced concrete structures” – Final Report, edited by R. Cigna, C. Andrade, U. Nürnberger, R. Polder, R. Weydert and E. Seitz, 2003.

[9] B. Sørenson, P. B. Jensen and E. Maahn: “The corrosion properties of stainless steel reinforcement” in “Corrosion of reinforcement in concrete” edited by C. L. Page, K. W. J. Treadaway, P. B. Bamforth, Elsevier Applied Science, 1990.

[10] HIPER Project: “Increased infrastructure reliability by developing a low cost and high performance stainless steel rebars” - GDR1-2000-25601 from EC.